2016

Spatiotemporal Distribution of the Himalayan Leucogranite: Implications for Mountain-building as a Function of Indian Slab Dynamics

Hongcheng Guo
Louisiana State University and Agricultural and Mechanical College

SPATIOTEMPORAL DISTRIBUTION OF THE HIMALAYAN LEUCOGRANITE: IMPLICATIONS FOR MOUNTAIN-BUILDING AS A FUNCTION OF INDIAN SLAB DYNAMICS

A Thesis

Submitted to the Graduate Faculty of the
Louisiana State University and
Agricultural and Mechanical College
in partial fulfillment of the
requirements for the degree of
Master of Science

in

The Department of Geology and Geophysics

by
Hongcheng Guo
B.Eng., Hefei University of Technology, 2014
August 2016

ACKNOWLEDGEMENTS

I extend the sincerest appreciation to my advisor, Dr. Alex Webb, for his encouragement, enthusiasm, and constructive criticism. Without his patience, insights, and helpful discussion, I could not have finished this project and progressed my scientific thinking.

I greatly appreciate the support, guidance, and time Dr. Peter Clift and Dr. Juan Lorenzo provided. Their advice on the early manuscript and on my exam was truly helpful.

I also appreciate Dr. Jess King, from University of Hong Kong, who provided insightful help on crustal anatexis mechanisms, which greatly improve the manuscript. I also thank Dr. Jess King for her advice and help on the educating me with geochemistry, which I would like to employ for the further research of this project.

I thank my graduate faculties and graduate peers who shared these two years with me. I learned a lot on how to being a good researcher and a good man from the interaction with them.

Finally, I give the special thank my parents, Jiaming Wang and En'hui Zhai, for the love, support, and sacrifice they ever made to my education and to my life. Without them, I could not have started my graduate study.

TABLE OF CONTENTS

LIST OF TABLES

LIST OF FIGURES

ABSTRACT

The Himalayan orogen, as a natural laboratory for continental collision, has attracted intense research attention for decades. However, the question of how the orogen was built is still debated, and potential answers are few when considering how and why along-strike variations of the mountain-building processes occurred. Various tectonic models have been proposed to explain the kinematics of the mountain-building. These models include two dimensional models, such as wedge extrusion (Burchfiel and Royden, 1985; Grujic et al., 1996; Kohn, 2008), channel flow coupled to focused denudation (Beaumont et al., 2001; Hodges et al., 2001), tectonic wedging (Yin, 2006; Webb et al., 2007), duplexing (He et al., 2015; Larson et al., 2015), and a recently proposed three dimensional model in which lateral migration of Indian slab detachment controlled the mountain building (Webb et al., submitted). Here, these models are tested by examining which model(s) can explain the generation of the leucogranites that occur along the orogen. The two-dimensional models predict that leucogranite ages and distributions should not vary significantly along the length of the orogeny, whereas the three-dimensional slab detachment model predicts that leucogranite generation should vary along-strike in specific ways, most notably by showing increasingly young minimum ages of large leucogranite bodies towards the east-central Himalaya. We compiled the existing geochronological data sets and estimated the volume of Himalayan leucogranites, revealing (1) increasing volumes and younging of leucogranite bodies from the ends of the orogen towards the east-central Himalaya, and (2) that younger leucogranite bodies appear generally larger than older emplaced bodies in any given range sector. These findings are generally consistent with the predictions of the lateral migration of slab detachment model, indicating that this model offers a viable explanation for the spatiotemporal distribution of Himalayan leucogranite. This interpretation prompts a re-

evaluation of pre-existing two-dimensional models and confirms that Himalayan mountain building proceeded largely via duplexing, as modulated in three dimensions and time by the dynamics of the subducting Indian plate.

CHAPTER 1. INTRODUCTION

Cenozoic convergence of India and Eurasia produced the Himalayan orogen along the collisional front, providing a natural laboratory for studying continent-continent collision. A major, long-standing question here is how did the Himalayan orogen develop? Different hypotheses have been proposed to answer this question. Models include: wedge extrusion (Burchfiel and Royden, 1985; Grujic et al., 1996; Kohn, 2008), channel flow coupled focused denudation (Beaumont et al., 2001; Hodges et al., 2001), tectonic wedging (Yin, 2006; Webb et al., 2007), duplexing (He et al., 2015; Larson et al., 2015), and lateral migration of slab detachment (Webb et al., submitted). Wedge extrusion models regard the crystalline core of the orogen (commonly specified as the Greater Himalayan Crystalline complex) as a northwards-tapered wedge extruding southwards between two low-grade sequences (the Tethyan Himalayan Sequence above, and the Lesser Himalayan Sequence below) (Burchfiel and Royden, 1985; Grujic et al., 1996). Channel flow coupled to focused denudation models envision Greater Himalayan Crystalline complex emplacement as a product of southwards flow of partially molten crust which was driven out by the gravitational potential of the topographically high Tibetan plateau during the Eocene to Oligocene and then coupled to climate-modulated erosion and exhumed along a narrow steep range during the Early Miocene to Middle Miocene (Beaumont et al., 2001, 2004; Hodges et al., 2001; Godin et al., 2006a). Tectonic wedging models show emplacement of the Greater Himalayan Crystalline complex at depth along the Main Central thrust (Yin, 2006; Webb et al., 2007). In this interpretation the South Tibetan detachment is a backthrust that reaches the surface to the north as the Great Counter thrust, in contrast to the prior models in which this was considered a normal fault. Duplexing models are similar to the tectonic wedging model, but show that thrust sheets continuously accreted at depth

to form the bulk of the Greater Himalayan Crystalline complex/duplex, as evidenced by abundance of recently published evidence for thrust faults stacking layers that experience roughly consistent metamorphic cycles at progressively younger periods to the south (Corrie and Kohn, 2011; Carosi et al., 2010; Montomoli et al., 2013; Imayama et al., 2012; Rubatto et al., 2013; Ambrose et al., 2015; Larson et al., 2015). Finally, a three-dimensional model involving lateral migration of Indian slab detachment proposed that the Himalayan mountain-building phases are partitioned by Indian slab underthrusting, rollback, and detachment (Webb et al., submitted). As these processes are non-uniform in time and space, they are proposed to similarly impose three-dimensional heterogeneity upon Himalayan crustal evolution. The main development of the Greater Himalayan Crystalline complex/duplex in this model is thought to occur in response to slab rollback and resultant steepening. The slab steepening would in turn steepen the orogenic decollement and thus via standard wedge mechanics (e.g., critical taper Coulomb wedge models like Davis et al., 1983) encourage thickening and duplexing.

To evaluate which hypothesized model(s) can explain Himalayan mountain building, we compare their predictions versus compiled data sets for distinctive young igneous rocks of the Himalayan system, the famous Himalayan leucogranites (e.g. Harrison et al., 1997). Because these rocks developed during Cenozoic Himalayan orogenesis, the integrated age and distribution of these rocks can be used as a sensitive recorder of the tectonic evolution. The tectonic models described above make a number of predictions relevant to leucogranite generation. The most distinctive prediction is that the two-dimensional models are only capable of describing arc-perpendicular and vertical variations across the Himalaya, whereas the slab dynamics model also offers arc-parallel distinctions which track slab processes that varied along the strike of the orogen, such as break-off (e.g. Replumaz et al., 2010). Below these predictions

are detailed, with analysis focusing on how the proposed tectonic evolution should generate different patterns of crustal anatexis and leucogranite production. Furthermore, the predictions are tested via compilation and filtering of Himalayan leucogranite data, primarily focusing on leucogranite volumetric, and chronological distribution. Clear arc-parallel variability in leucogranite production emerges, requiring three-dimensional models of Himalayan orogenesis.

CHAPTER 2. HIMALAYAN OROGENY AND LEUCOGRANITE GENESIS

2.1 Himalayan Orogeny

Himalayan orogen (Figure 1) has been built as the collisional product of the India and Eurasia. The orogen comprises four tectonostratigraphic units. They are, from north to south: (1) the Tethyan Himalayan Sequence (THS) composed of Proterozoic to Eocene (meta-) sedimentary rocks; (2) the Greater Himalayan Crystalline complex (GHC) composed of Paleoproterozoic to Ordovician inverted high-grade metamorphic rocks; (3) the Lesser Himalayan sequence (LHS) composed of Proterozoic to Cambrian low-grade (meta-) sedimentary rocks; (4) sub-Himalayan Sequence, late Cretaceous to Tertiary foreland basin rocks (Le Fort, 1975; Hodges, 2000; Godin et al., 2001; Yin , 2006). The South Tibetan detachment (STD), the Main Central thrust (MCT), and the Main Boundary thrust (MBT) separate the four units, from north to south. To the north these units are bounded by the Indus-Yarlung suture

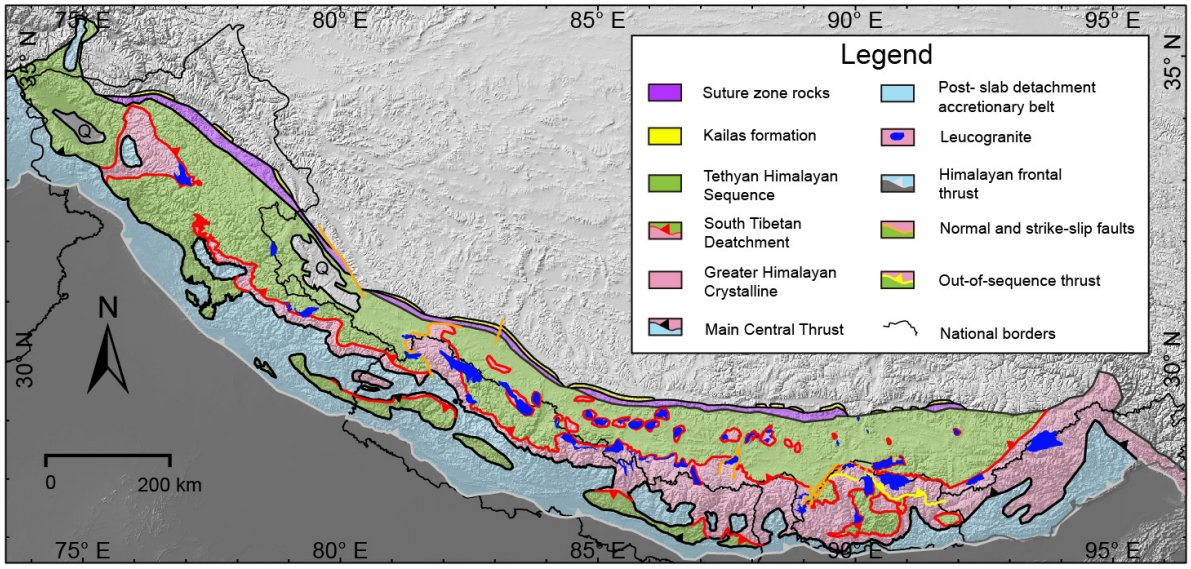

Figure 1. Simplified geological map of Himalaya. The map shows main tectonic units, faults, and main leucogranite bodies. Some leucogranite without sufficient volume to be plotted as distinct bodies are no shown. Modifies from Aitchison et al. (2002, 2007), An et al. (2014), Ding et al. (2005), Greenwood et al. (2016), Grujic et al. (2011), He et al. (2015), Henderson et al. (2011), Kellett and Grujic (2012), Pan et al. (2004), Regis et al. (2014), Thakur and Rawat (1992), Webb et al. (2011), Yan et al. (2012), and Yu et al. (2015).

zone (IYSZ), the southern limit of which is commonly defined by the south-dipping Greater Counter thrust (Yin et al., 1994, 1999).

Different hypotheses of tectonic models have been proposed to explain the development of the Himalayan orogen, including wedge extrusion (Burchfiel and Royden, 1985; Grujic et al., 1996; Kohn, 2008), channel flow coupled focused denudation (Beaumont et al., 2001; Hodges et al., 2001), tectonic wedging (Yin, 2006; Webb et al., 2007), duplexing (He et al., 2015; Larson et al., 2015), and lateral migration of Indian slab detachment (Webb et al., submitted). Each of these models is described below.

2.1.1 Wedge Extrusion

In this model (Figure 2), the Greater Himalayan Crystalline complex was derived from the Indian crust and is regarded as a wedge extruding southward between the lower grade

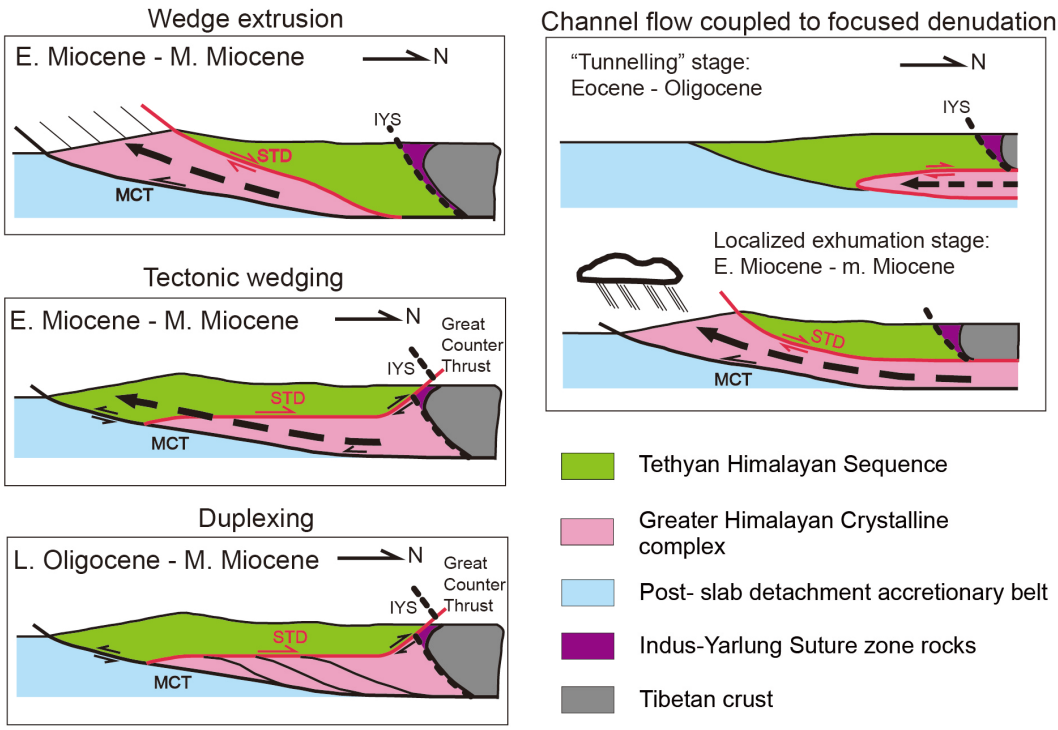

Figure 2. Two-dimensional tectonic models illustrating the Himalayan mountain-building. MCT: Main Central thrust; STD: South Tibetan detachment; IYS: Indus-Yarlung suture. Modified from Webb et al. (2011).

Tethyan Himalayan Sequence and Lesser Himalayan Sequence bounded above by the South Tibetan detachment and below by the Main Central thrust. The South Tibetan detachment is thus a north-dipping normal fault that may be driven by upper-crustal extension along the range crest (Burchfiel and Royden, 1985). A similar Coulomb wedge model explains that the South Tibetan detachment may be an adjustment to maintain critical taper as local gravitational collapse (Burg et al., 1984; Robinson et al., 2006; Kohn, 2008). The model predicts a coeval motion of the Main Central thrust and the South Tibetan detachment and a down-dip merger of these two faults.

2.1.2 Channel Flow Coupled to Focused Denudation

In the earlier version of this model, the rocks of the Greater Himalayan Crystalline complex were derived from the Asian crust and regarded as the product of the partially molten Asian crust (Nelson et al., 1996), whereas later versions of this model permit that these rocks could have been stripped from the subducting Indian plate (Beaumont et al., 2001). It is predicted that the gravitational potential of the topographically high Tibetan plateau drives the Greater Himalayan Crystalline complex rocks southwards, forming a low-viscosity "tunnel" or channel (Beaumont et al., 2001, 2004; Godin et al., 2006a). Bounded by the active Main Central thrust and South Tibetan detachment, the channel is locally exhumed by erosion where focused precipitation results from the orography of the topographic front during the Early and Middle Miocene (Beaumont et al., 2001; Hodges et al., 2001). The south Tibetan detachment thus acts as a normal fault in this model, as in the wedge extrusion model. The channel flow model likewise predicts a coeval motion of the Main Central thrust. The Main Central thrust and the South Tibetan detachment are predicted to be subparallel and extend beneath Tibet north of the Indus-Yarlung suture.

2.1.3 Tectonic Wedging

This model was inspired by the discovery of the leading edge of the Greater Himalayan Crystalline core, i.e., that the Main Central thrust and the South Tibetan detachment merge to the south along the Himalaya (Thakur, 1998; Yin, 2006; Webb et al., 2007). Instead of either predicting an exposed or exhumed Greater Himalayan Crystalline complex, this model considers it to lie entirely beneath the Tethyan Himalayan Sequence (Yin, 2006, Webb et al., 2007). Rather than consider the South Tibetan detachment as extensional fault, tectonic wedging model kinematically links it to the Great Counter thrust and regards it as a back thrusting in the Main Central thrust hanging wall.

2.1.4 Duplexing

Duplexing is similar to tectonic wedging except that this model shows thrust sheets continuously accreted at depth to form the bulk of the Greater Himalayan Crystalline complex/duplex (He et al., 2015; Larson et al., 2015). The south Tibetan detachment is seen as the roof backthrust that accommodates the duplex development. This model is based on (1) the abundance of recently published evidence for thrust faults stacking layers that experience roughly consistent metamorphic cycles at progressively younger periods to the south within the Greater Himalayan Crystalline complex (Corrie and Kohn, 2011; Carosi et al., 2010; Montomoli et al., 2013; Imayama et al., 2012; Rubatto et al., 2013; Ambrose et al., 2015; Larson et al., 2015) and (2) the southwards merger of the Main Central thrust and South Tibet detachment, as in the tectonic wedging model (Webb et al., 2007; described above). The model predicts that thrust sheets were accreted to the lower portion of Greater Himalayan Crystalline. The process repeated and propagated from north to south, thus building the Greater Himalayan Crystalline duplex.

2.1.5 Lateral Migration of Indian Slab Detachment

Recently, a new three-dimensional model (Figure 3) proposes that the detachment of the subducted Indian slab and its lateral migration controlled the Himalayan mountain building (Webb et al., submitted). This model shows that the Indian slab underthrusted the Asian plate prior to ca. 30 Ma. From ca. 30 Ma to ca. 25 Ma, Indian slab rolled back. After the rollback and prior to the slab detachment, the Greater Himalayan Crystalline core grew via duplexing. The Indian slab then broke off at both ends of the Himalaya ca. 25 Ma, and the crack tip allowing slab detachment subsequently migrated towards the eastern-central Himalaya. The break-off finally was completed ca. 15 Ma to 8 Ma in the east-central Himalaya.

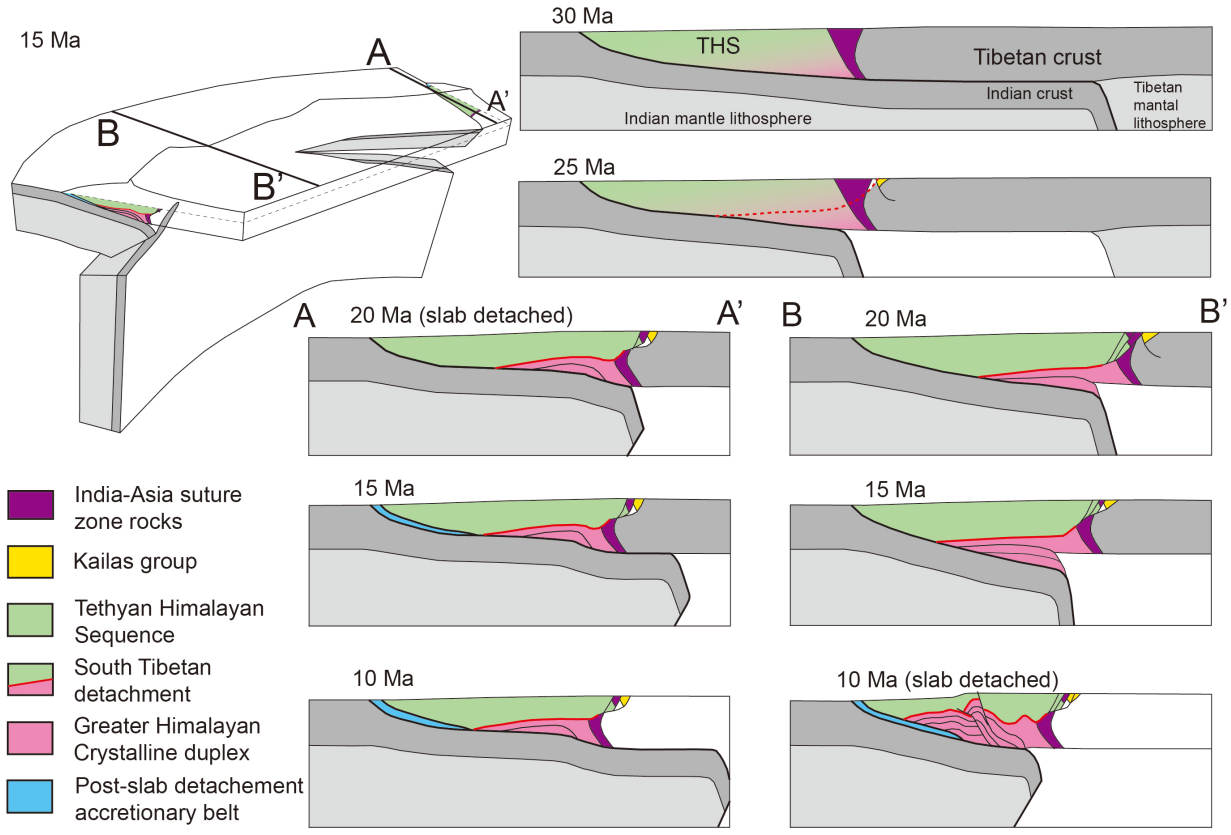

Figure 3. Three-dimensional model illustrating the Himalayan mountain-building. Modified from Webb et al. (submitted).

2.2 Leucogranite Genesis

To examine which model(s) can Himalayan mountain building, Comparison of their predictions (in Section 3) versus compiled data sets for distinctive young igneous rocks of the Himalayan system, the famous Himalayan leucogranites (e.g. Harrison et al., 1997), is made. Because these rocks developed during Cenozoic Himalayan orogenesis, the integrated age and distribution of these rocks can be used as a sensitive recorder of the tectonic evolution.

The Himalayan leucogranite occurs along the orogen as a discontinuous belt. The leucogranite is mostly exposed as plutons, dikes, and veins. They are either intruded into the high grade rocks at the top of the Greater Himalayan Crystalline core along the South Tibetan detachment (here, these are named Greater Himalayan leucogranite), or intruded in the series of Higher Himalayan genesis domes in the Tethyan Himalayan Sequence (here, these are named North Himalayan leucogranite).

Leucogranite generation is thought to have been caused by the partial melting of crust. There are essentially two kinds of crustal anatexis, including vapor-present anatexis (Figure 4) and vapor-absent anatexis (Figure 5), which either lower the solidus temperature or raise the local geothermal gradient. Vapor-present anatexis occurs by addition of volatile components, such as H_2O and CO_2 when the resultant partial melted portion of crust is deep enough to trigger metamorphism through dehydration and decarbonation reactions. Therefore, vapor-present anatexis can occur as burial proceeds. However, vapor-absent anatexis can happen during shear heating and/or decompression by raising temperature and/or lowering pressure of the crust. Below, existing anatexis models proposed for the Himalayan leucogranite genesis are reviewed.

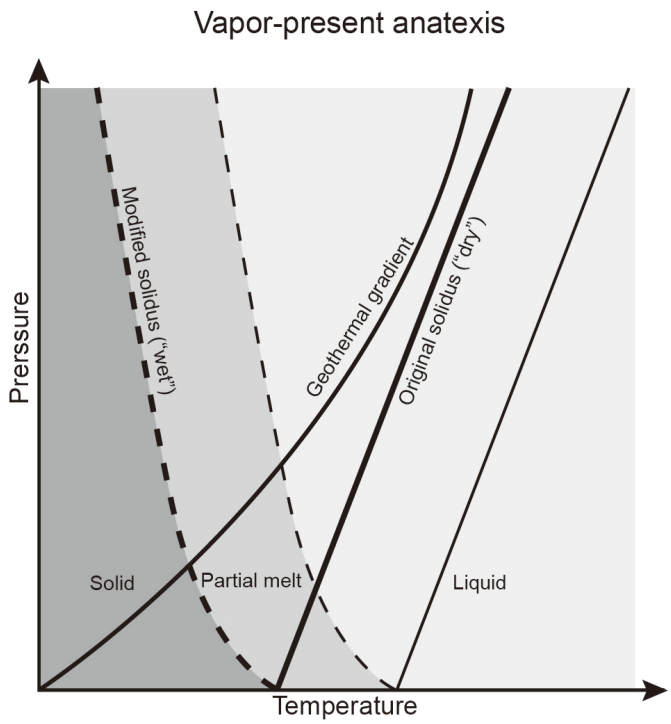

Figure 4. Pressure-temperature space diagram of vapor-present anatexis.

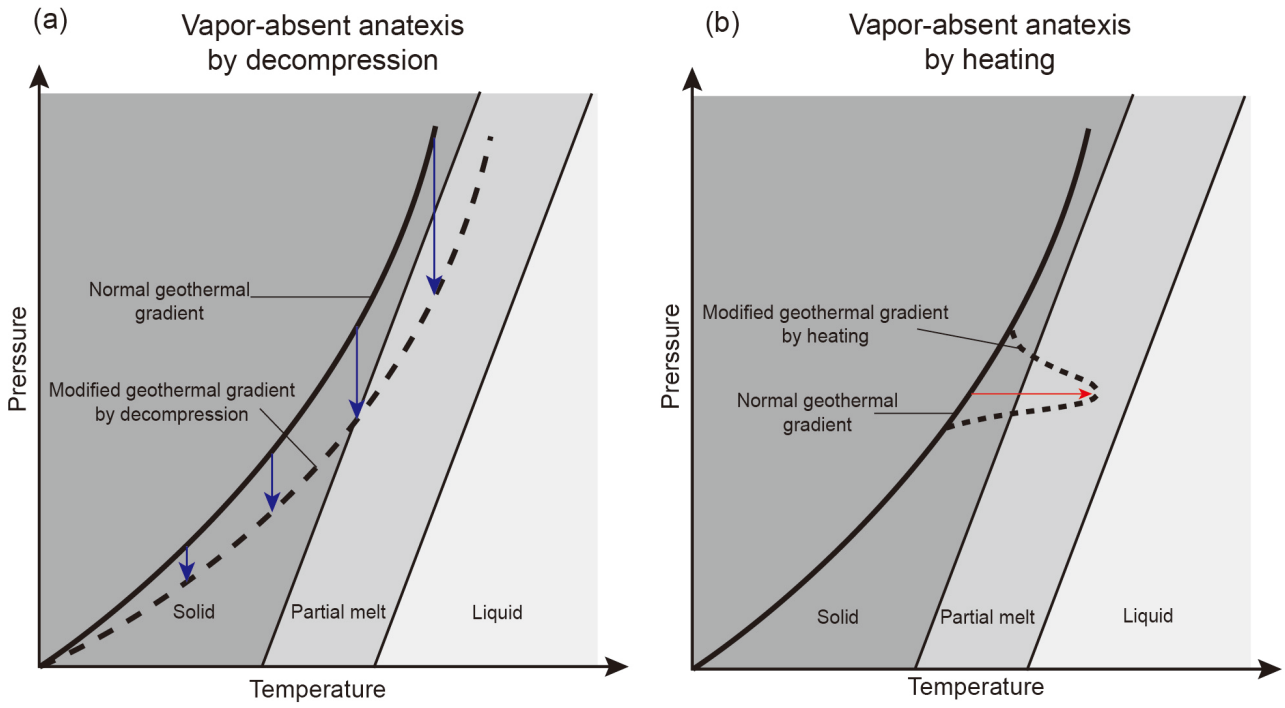

Figure 5. Pressure-temperature space of vapor-absent anatexis.

2.2.1 Vapor-present Anatexis

2.2.1.1 “Hot Iron” Melting

This model is proposed to explain the chain of the thrusting on the Main Central thrust, the inverted metamorphism of the Greater Himalayan Crystalline core, the fluid release and crustal partial melting, and the generation and emplacement of the Himalayan leucogranite. This model proposes that the deep hot Tibetan slab is continuously moved over the low grade Lesser Himalayan Sequence due to the thrusting of the Main Central thrust. The thermal relaxation following thrusting along the MCT heated the footwall to produce dehydration reactions. The top-to-bottom heating induced by the thrusting also resulted in the inverted metamorphism. The dehydration and decarbonation metamorphic reactions of the footwall rocks release H_2O and CO_2 fluids that are introduced into the hot hanging-wall. They trigger the partial melting of the hanging wall Greater Himalayan Crystalline core by fluxing gneisses and thus produce the leucogranite melts. The melts emplace via giant dykes to the higher structure level of the Greater Himalayan Crystalline core (Le Fort, 1975, 1981, 1986, 1987; Vidal et al., 1982).

This model has been criticized for requiring high hanging wall temperature along the ramp during thrusting because Harrison et al. (1999b) noted that the melting of Greater Himalayan Crystalline is not temporally related to the recrystallization of Lesser Himalayan Sequence. The necessity of fluid existence for melting was questioned by the finding that the Rb/Sr rations of Himalayan leucogranites are too high to be related to their assumed Greater Himalayan Crystalline source rocks (Thompson, 1982; Harris et al., 1993) and the finding that fluid-present melting in similar settings (Patiño Douce and Harris, 1998) yield melts with compositions that are different from the Himalayan leucogranite.

2.2.1.2 Burial Heating

Based on thermodynamic approaches, including microstructures, mineral compositions and P-T evolution, conducted in Barun Gneiss from the Greater Himalayan Crystalline core of eastern Nepal, Groppo et al. (2012) proposes that burial heating mainly results in the melt production and that decompressional process does not considerably contribute to the whole production.

2.2.2 Vapor-absent Anatexis

2.2.2.1 Radioactive Heating

Following the finding of high U and Th concentration of the Himalayan gneisses, Molnar et al. (1983) proposes that radioactivity could provide a heat source for melting after decades of continental subduction. This idea was later revised to involve radioactive crust accretion on the MCT hanging-wall coupled with focused erosion (Royden 1993; Huerta et al., 1996).

2.2.2.2 Shear Heating

This model attributes the heat source to shear heating from stresses along the MCT in the range 100-1100 MPa (England et al., 1992; England and Molnar, 1993). It has been criticized because the shear stresses required for melting in this model may exceed a maximum value for ductile shearing by a few tens of MPa, and thus may not by sustainable in ductile shear zone (Harrison et al. 1999b).

2.2.2.3 Decompression Melting

It has been proposed that most Himalayan anatexis occurred due to fluid absent reactions instead of fluid-presenting melting (Harris and Inger, 1992; Harris et al, 1993; Harris and Massey, 1994; Patiño Douce and Harris, 1998) via trace element modeling and experimental petrology. Harris and Massey (1994) argue that the melting was triggered by decompression resulting from

slip on the STD (interpreted as a normal fault) instead of by heating. This model relates the anatexis to the slips on the STD instead of the thrusting of the MCT. The uplift and exhumation resulted in decompression of the Greater Himalayan Crystalline core, and thereby triggered the melting.

2.2.3 Summary

Taking the fundamental mechanisms for partial melting and the above existing models discussed above together, regardless of their strength and weakness, we conclude that the following mechanisms could have produced the crustal anatexis necessary for the Himalayan leucogranite generation: vapor-present anatexis and vapor-absent anatexis. Vapor-present anatexis can occur in Himalayan low crust in setting of burial when crust is thickened enough. Metamorphism occurs, and dehydration and decarbonation reactions release vapor. Decreased solidus temperature in response to the H_2O and CO_2 flux therefore allows crustal partial melting and produced a small volume of leucogranite magma. Vapor-absent anatexis can be triggered by prograde shear heating and retrograde decompression. Heat produced by friction along the Main Central thrust rises up the local geothermal and therefore initiates crustal partial melting. Decompression, in response to either extrusion/duplexing of the Greater Himalayan Crystalline complex/duplex or rapid uplift and exhumation resulted from Indian slab detachment, is able to trigger larger volume of partial melting.

CHAPTER 3. PREDICTIONS OF TECTONIC MODELS ON MELTING PROCESS

Here, predictions of the spatial, volumetric, and temporal distribution of leucogranite that may be produced in each of the proposed Himalayan tectonic evolution mechanisms (described in the previous chapter) are explained in order to provide a framework for model testing. Every model predicts different leucogranite volumes produced at different stages, but none of the two-dimensional models predict lateral variations in timing and volume. Only the three-dimensional model involving lateral migration of slab detachment supplies varying along-strike predictions.

The wedge extrusion model (Figure 6) regards the Greater Himalayan Crystalline complex a north-taped wedge extruding southwards between the Tethyan Himalayan Sequence and Lesser Himalayan Sequence (Burchfiel and Royden, 1985; Grujic et al., 1996). This model predicts that melting may result from (1) early burial heating prior to the extrusion, (2) shear heating along the Main Central Thrust and (3) decompression during the wedge extrusion. The first two methods are prograde heating, and the third method is retrograde decompression.

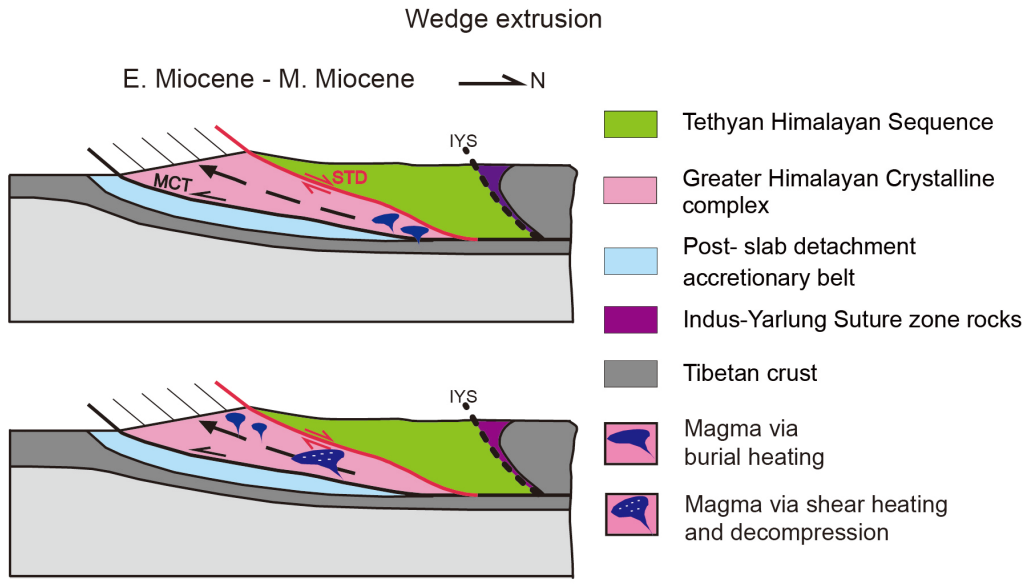

Figure 6. Predictions of melting process of the wedge extrusion model.

Channel flow coupled to focused denudation model (Figure 7) envisions the Greater Himalayan Crystalline core as the product of partially molten Asian crust that flows southwards by gravitational potential of the topographically high Tibetan plateau (Beaumont et al., 2001, 2004; Godin et al., 2006a) during Eocene to Oligocene and is locally exhumed by erosion during Early Miocene to Middle Miocene (Beaumont et al., 2001; Hodges et al., 2001). This model predicts that a small amount of melting may result from (1) early burial heating during "tunneling" stage, (2) shear heating along the Main Central thrust and (3) decompression via the exhumation of Greater Himalayan Crystalline during localized exhumation stage. The first two methods are prograde heating, and the third method is retrograde decompression.

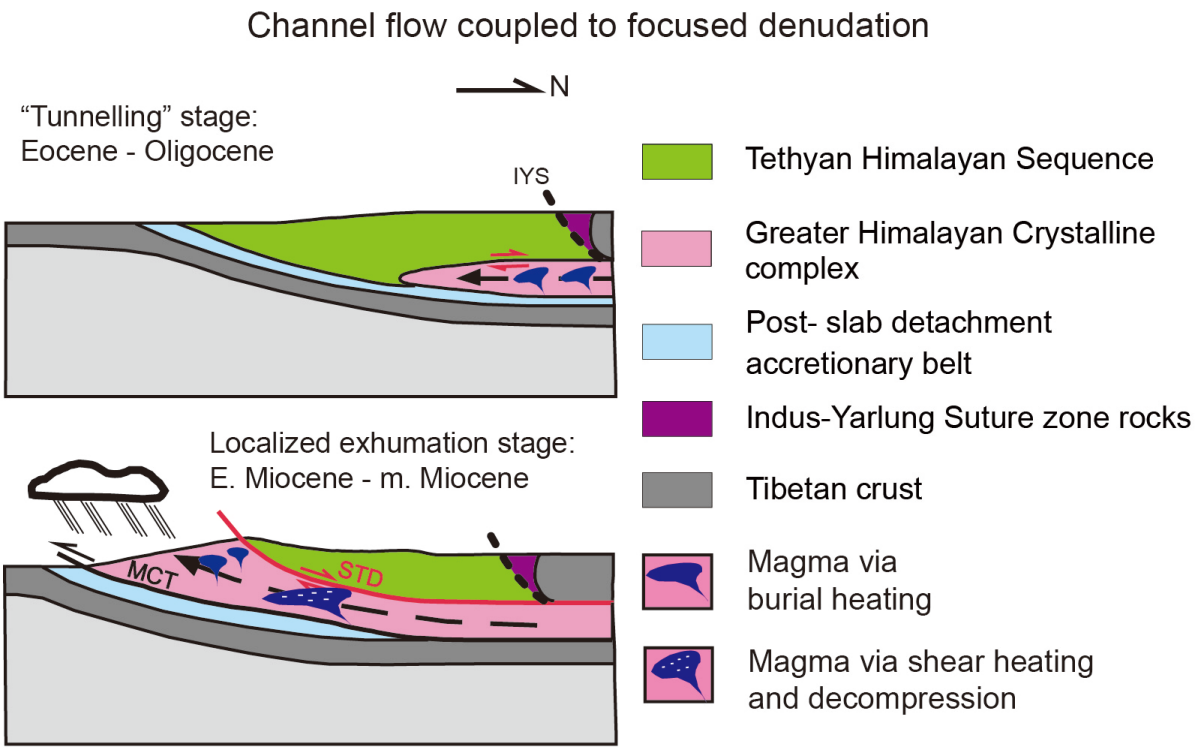

Figure 7. Predictions of melting process of the channel flow coupled to focused denudation model.

Tectonic wedging model (Figure 8) shows the South Tibetan detachment as a backthrusting that kinematically links to the Great Counter thrust (Yin et al., 1999). The model shows

emplacement of the Greater Himalayan Crystalline core at depth bounded by the Main Central thrust and the South Tibetan detachment that merge to the south (Webb et al., 2007). This model predicts that melting may result from (1) early burial heating, (2) shear heating along the Main Central and (3) decompression during the uplift and exhumation of Greater Himalayan Crystalline complex. The first two methods are prograde heating, and the third method is retrograde decompression.

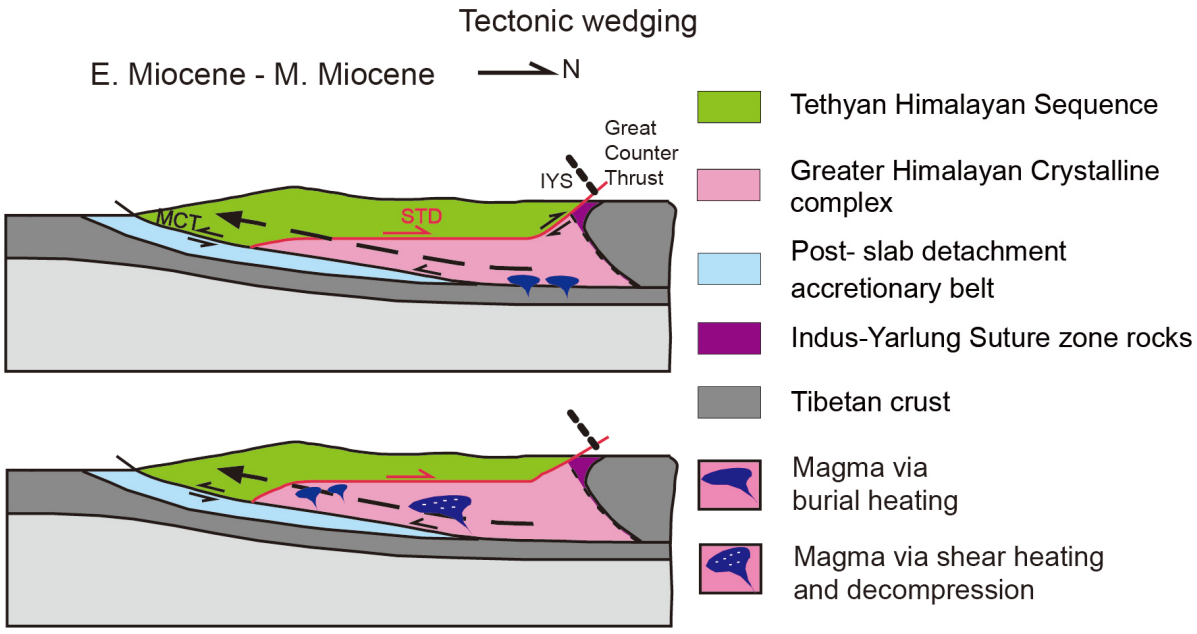

Figure 8. Predictions of melting process of tectonic wedging model.

Duplexing model (Figure 9) proposed that thrust sheets continuously accreted at depth to form the bulk of the Greater Himalayan Crystalline complex/duplex (He et al., 2015; Larson et al., 2015). In this model, we have similar prediction that melting can result from (1) early burial heating, (2) shear heating along the Main Central thrust via shear heating and (3) decompression via the duplexing of Greater Himalayan Crystalline duplex. The first two methods are prograde heating, and the third method is retrograde decompression.

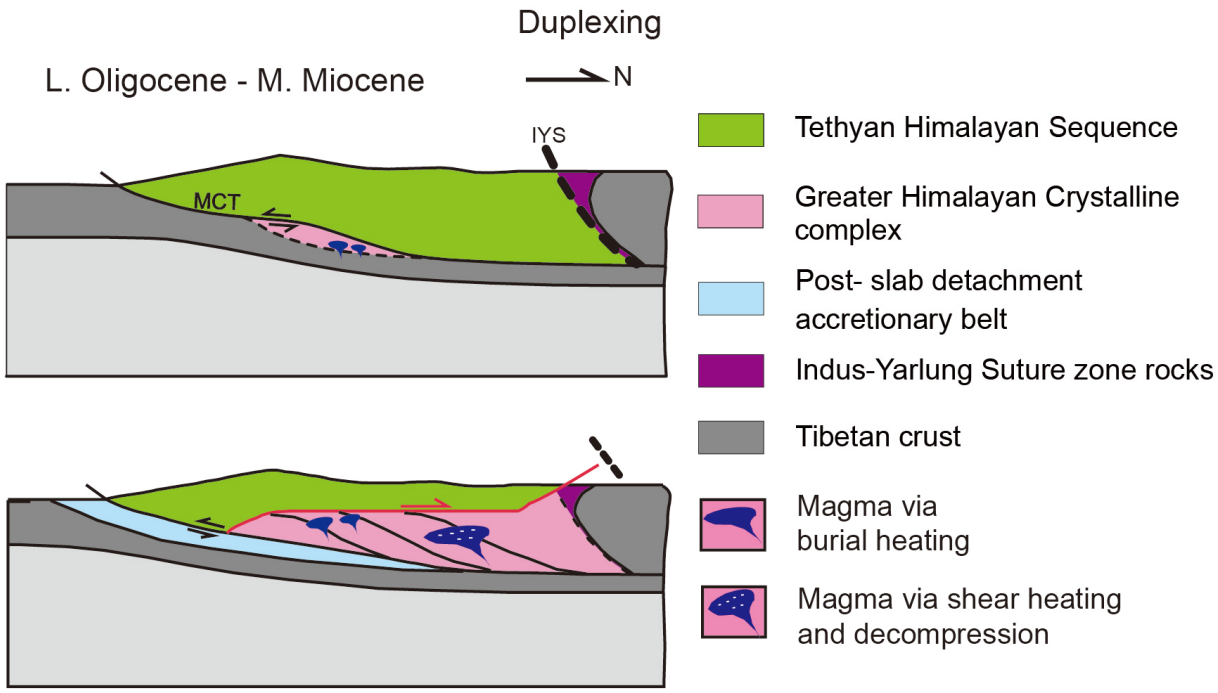

Figure 9. Predictions of melting process of duplexing model.

The lateral propagation of slab detachment model (Figure 10) predicts that Himalayan leucogranite was generated by the following processes: (1) deep burial produced heating that triggered melting of the deep crust and thus a small volume of melts was produced by prograde vapor-present heating before the slab rollback; (2) shearing heating along the thrust sheets and decompression in response to the duplexing of the weakened crust and exhumation produced moderate melting during the period after the slab rollback and before the slab detachment; (3) slab detachment produced relatively large-volume melting in response to rapid decompression during the rapid uplift and exhumation resulting from the isostatic rebound of the orogen. Controlled by the Indian slab dynamics, these processes occurred in different time along the orogen. Above predictions were summarized in Table 1 and Figure 11.

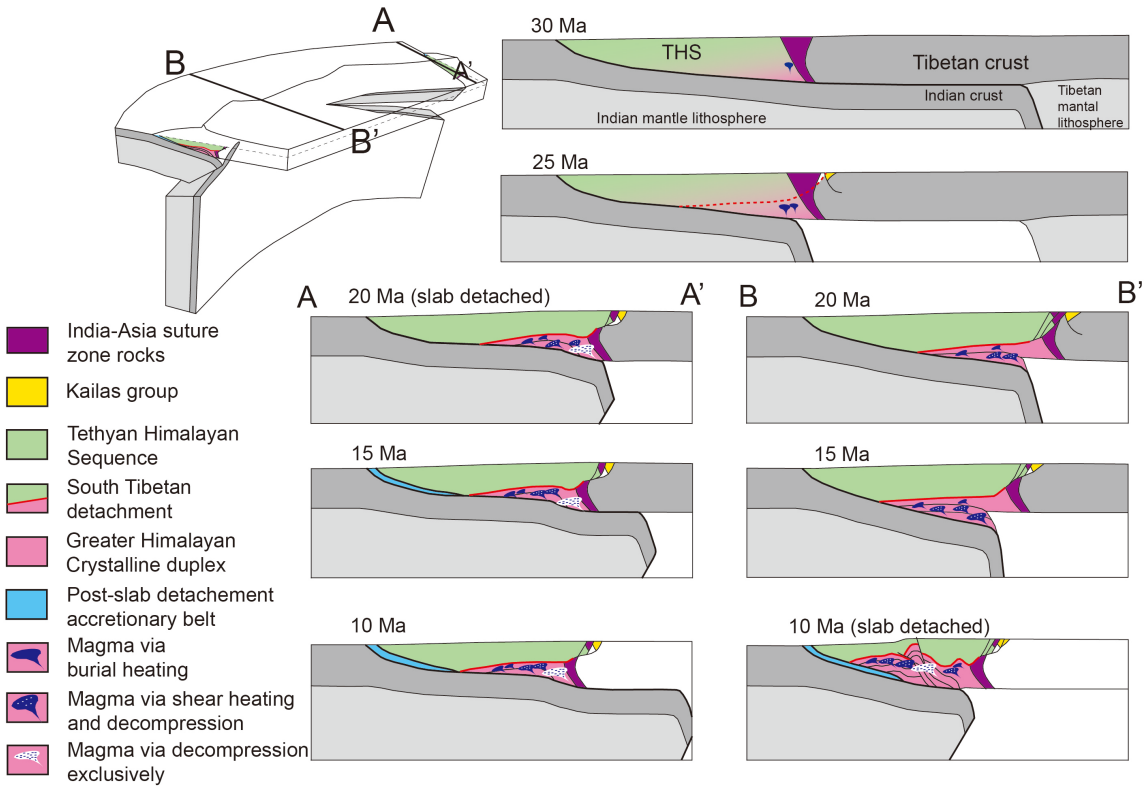

Figure 10. Prediction of melting process of the three-dimensional slab detachment model. Modified from Webb et al. (submitted).

Table 1. Examination of the compatibilities of petrogenetic models and tectonic models and predictions on the timing and volume of Himalayan leucogranite.

Tectonic models	Timing	Burial heating	Shear heating	Decompression	Volume prediction	Illustration
Wedge extrusion	Eocene to Oligocene pre-extrusion	√			Small	Figure 11(a)
	E. Miocene to M. Miocene		√	√	Modest	
Channel flow coupled to focused denudation	Eocene to Oligocene "tunnelling"	√			Small	Figure 11(a)
	E. Miocene to M. Miocene exhumation		√	√	Modest	
Tectonic wedging	Eocene to Oligocene pre-wedging	√			Small	Figure 11 (a)
	E. Miocene - M. Miocene		√	√	Modest	
Duplexing	Eocene - L. Oligocene pre-duplexing	√			Small	Figure 11 (b)
	L. Oligocene - M. Miocene		√	√	Modest	

(Table 1 continued)

Tectonic models	Timing	Burial heating	Shear heating	Decompression	Volume prediction	Illustration
Lateral migration of slab detachment	Eocene - E. Oligocene underthrusting	√			Small	Figure 11 (c)
	E. Oligocene - L. Oligocene slab rollback	√			Small	
	L. Oligocene - Miocene duplexing	√	√	√	Modest	
	Miocene slab detachment			√	Large	

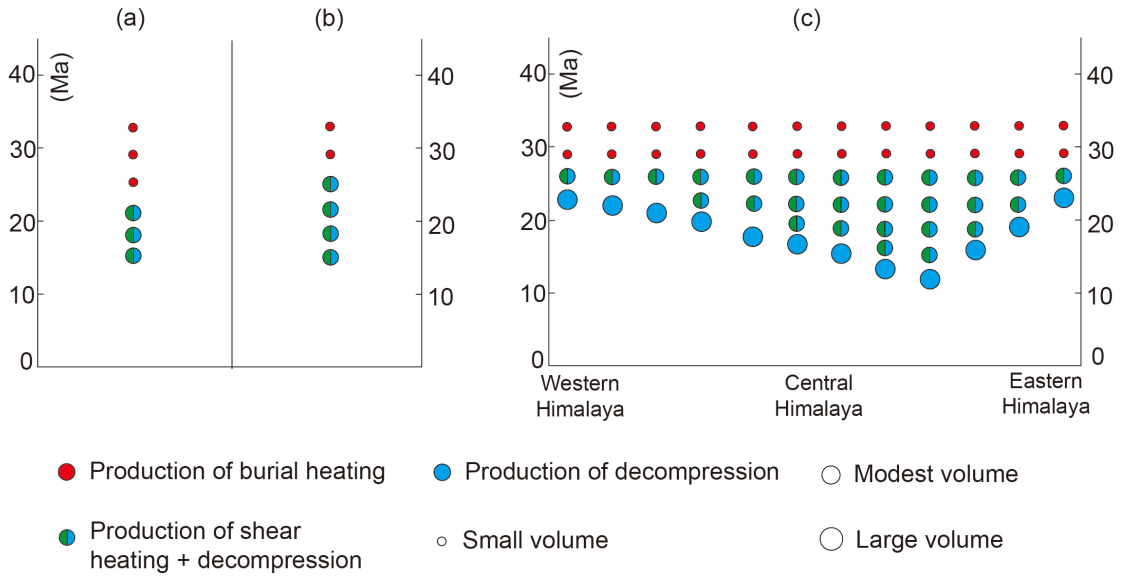

Figure 11. Conceptual diagram of model predictions on timing and volume of the Himalayan leucogranite. (a) Prediction of the wedge extrusion model, channel flow coupled to focused denudation model, and tectonic wedging mode. (b) Prediction of the duplexing model. (c) Prediction of the three-dimensional slab detachment model. The size of circles represents the relative leucogranite volume at different periods. Note that the amount of the circles does not necessarily indicate the real episodes of melting pulses.

CHAPTER 4. TESTS

Here, we test the predictions made by these tectonic models via the compilation and filtering of Himalayan leucogranite data, primarily focusing on leucogranite volumetric, and chronological distribution.

4.1 Geochronology

A large amount of geo- and thermo- chronological work has been conducted to explore the age of the Himalayan leucogranite bodies. Initially, Ar-Ar, K-Ar, and Bb-Sr isotopic systems have been used. However, their inaccuracy with low closure temperatures or susceptibility to contamination or alteration usually generates unreliable crystallization ages for leucogranite. Instead, U-(Th-)Pb isotopic system has now been widely used for dating zircon, monazite, and xenotime grains in leucogranite. Here, published crystallization ages of leucogranite bodies in the high structural level of GHC and leucogranite bodies exposed in THS gneiss domes along the Himalayan orogen are presented (Table 2).

Figure 12 presents several kinds of age pattern for a single dated leucogranite. For homogenous age population (as evidenced by low MSWD), the weighted mean of the total population is interpreted to represent the emplacement age. For discontinue heterogeneous age population, the youngest weighted mean of multiple clusters represents the emplacement age (here, we use term “weighted mean of youngest U/Pb/Th age” in Table 2). For continuous heterogeneous age population, some published chronological data sets provide the weighted mean of selected young populations (here, we use term “youngest weighted mean age” in Table 2). Unfortunately, many geochronological data sets only provide a weighted mean of total age population in cases with heterogeneous age populations (as evidenced by high MSWD). In these circumstances, interpretation that the weighted mean ages do not post the leucogranite

Table 2. Compilation of the location, age and estimated area of the Himalayan leucogranite. Longitude values represent the locations of the centers of leucogranite bodies. Refer Figure 13 for longitude range for each leucogranite bodies. Estimated areas are calculated in ArcGIS under equal-area projection and are based on published geological mapping.

Region	Longitude (°)	Area (Km^2)	Timing (Ma)	Basis	References
Zanskar-Gianbul	77	589	20.6 – 19.5	U/Pb monazite ages	Noble and Searle, 1995
			21.2 ± 0.6	Mean of Th/Pb monazite ages	Horton et al., 2015
			22.1 ± 0.4	Mean of Th/Pb monazite ages	Horton et al., 2015
			21.3 ± 0.1	Weighted mean of U/Pb uraninite, xenotime, and zircon ages	Walker et al., 1999
			21.4 ± 0.1	Weighted mean of U/Pb uraninite ages	Walker et al., 1999
			22.1 ± 0.4	Weighted mean of U/Pb monazite ages	Walker et al., 1999
			22.2 ± 0.2	Weighted mean of U/Pb monazite ages	Dezes et al., 1999
			22.7 ± 0.9	Weighted mean of Th/Pb monazite ages	Robyr et al., 2006
			22.7 ± 0.9	Weighted mean of Th/Pb monazite ages	Robyr et al., 2006
			23.3 ± 0.9	Weighted mean of Th/Pb monazite ages	Robyr et al., 2006
			24.0 ± 0.3	Weighted mean of U/Pb monazite ages	Finch et al., 2014
			26.6 ± 0.2	Weighted mean of Th/Pb monazite ages	Robyr et al., 2006
Leo Pargil dome	78.7	205	17.9 ± 0.1	Weighted mean of Th/Pb monazite ages	Lerderer et al., 2013
			18.6 ± 0.1	Weighted mean of Th/Pb monazite ages	Lerderer et al., 2013
			19.0 ± 0.2	Weighted mean of youngest Th/Pb monazite ages	Lerderer et al., 2013
			19.0 ± 0.3	Weighted mean of youngest Th/Pb monazite ages	Lerderer et al., 2013
			19.1 ± 0.3	Weighted mean of youngest Th/Pb monazite ages	Lerderer et al., 2013
			19.2 ± 0.2	Youngest weighted mean of Th/Pb monazite ages	Lerderer et al., 2013

(Table 2 continued)

Region	Longitude (°)	Area (Km^2)	Timing (Ma)	Basis	References
			19.3 ± 0.2	Weighted mean of youngest Th/Pb monazite ages	Lerderer et al., 2013
			19.6 ± 0.1	Weighted mean of youngest Th/Pb monazite ages	Lerderer et al., 2013
			19.9 ± 0.1	Weighted mean of youngest Th/Pb monazite ages	Lerderer et al., 2013
			20.1 ± 0.3	Weighted mean of youngest Th/Pb monazite ages	Lerderer et al., 2013
			20.2 ± 0.2	Weighted mean of Th/Pb monazite ages	Lerderer et al., 2013
			20.7 ± 0.2	Youngest weighted mean of Th/Pb monazite ages	Lerderer et al., 2013
			21.7 ± 0.2	Weighted mean of Th/Pb monazite ages	Lerderer et al., 2013
			21.5 ± 0.2	Weighted mean of Th/Pb monazite ages	Lerderer et al., 2013
			21.8 ± 0.4	Youngest weighted mean of Th/Pb monazite ages	Lerderer et al., 2013
			~22	Mean of U/Pb zircon ages	Leech, 2008
			22.1 ± 0.3	Weighted mean of youngest Th/Pb monazite ages	Lerderer et al., 2013
			26.2 ± 0.2	Weighted mean of Th/Pb monazite ages	Lerderer et al., 2013
			29.0 ± 0.2	Weighted mean of Th/Pb monazite ages	Lerderer et al., 2013
Gangotri	78.7	74	22.4 ± 0.5	Weighted mean of Th/Pb monazite age	Harrison et al., 1997
Shivling	79.375	382	21.9 ± 0.5	Weighted mean of Th/Pb monazite age	Harrison et al., 1997
			23.0 ± 0.4	Weighted mean of youngest U/Pb monazite ages	Searle et al., 1999

(Table 2 continued)

Region	Longitude (°)	Area (Km^2)	Timing (Ma)	Basis	References
Bura Buru	82.475	227	23.6 ± 0.8	Weighted mean of U/Pb monazite ages	Carosi et al., 2013
Annapurna	84	< 10	22.1 + 0.6/-3.6	Weighted mean of U-Pb zircon ages	Hodge et al., 1996
Manaslu	84.65	442	17.6 ± 0.3	Single population of U/Pb monazite ages	Harrison et al., 1999
			19.3 ± 0.3	Weighted mean of U/Pb monazite ages	Harrison et al., 1999
			22.4 ± 0.5	Weighted mean of Th/Pb monazite ages	Harrison et al., 1995
			25 ± 0.5	U/Pb monazite ages	Deniel et al., 1987
Gyirong	85.35	477	~16.1	U/Pb monazite ages	Liao et al., 2003
			20.0 ± 1.7	Youngest weighted mean of U/Pb zircon ages	Zhang et al., 2012
			21.8 ± 1.3	Youngest weighted mean of U/Pb zircon ages	Zhang et al., 2012
Malashan	85.5	76	17.8 ± 2.2	Weighted mean of U/Pb zircon ages	Aoya et al., 2005
			17.6 ± 1.2	Youngest weighted mean of U/Pb zircon ages	Zhang JJ et al., 2012
			18.6 ± 5.6	Weighted mean of U/Pb zircon ages	Aoya et al., 2005
Paiku	85.65	309	19.3 ± 3.9	Weighted mean of U/Pb zircon ages	Kawakami et al., 2007
Shisha Pangma	85.8	336	17.3 ± 0.4	Weighted mean of U/Pb monazite ages	Searle et al., 1997
			20.2 ± 0.4	Weighted mean of U/Pb monazite ages	Searle et al., 1997
Xiaru	86.3	263	~35	Weighted mean of U/Pb zircon ages	Liu et al., 2015

(Table 2 continued)

Region	Longitude (°)	Area (Km^2)	Timing (Ma)	Basis	References
Nyalam	86.35	127	14.1 ± 1.4	Youngest weighted mean of U/Pb zircon ages	Wang et al., 2013
			16.8 ± 0.6	Weighted mean of U/Pb monazite ages	Scharer et al., 1986
Rongbuk	86.625	208	16.4 ± 0.1	Youngest weighted mean of Th/Pb monazite ages	Cottle et al., 2015
			22 ± 1	Weighted mean of Th/Pb monazite ages	Harrison et al., 1995
			21.6 – 20.6	U/Pb xenotime ages	Hodges et al., 1992
			16.4 ± 0.6	Weighted mean of Th/Pb monazite ages	Murphy and Harrison, 1999
			16.8 ± 0.8	Weighted mean of Th/Pb monazite ages	Murphy and Harrison, 1999
			15.6 ± 0.1	Weighted mean of Th/Pb monazite ages	Cottle et al., 2015
			15.4 ± 0.1	Weighted mean of Th/Pb monazite ages	Cottle et al., 2015
			15.3 ± 0.1	Weighted mean of Th/Pb monazite ages	Cottle et al., 2015
Everest	86.9	288	20.5 – 21.3	Youngest weighted mean of U/Pb monazite and xenotime ages	Simpson et al., 2000
			15.6 ± 0.2	Youngest weighted mean of U/Pb xenotime ages	Streule et al., 2010
			16.0 ± 0.6	Youngest weighted mean of U/Pb monazite ages	Streule et al., 2010
			16.1 ± 0.2	Youngest weighted mean of U/Pb monazite ages	Streule et al., 2010
			23.2 ± 0.8	Weighted mean of U/Pb zircon ages	Streule et al., 2010
			23.8 ± 0.2	Weighted mean of U/Pb zircon ages	Streule et al., 2010
			14.3 ± 0.6	Weighted mean of U/Pb monazite ages	Scharer et al., 1986
Lhagoi Kanri	87.45	91	15.1 ± 0.5	Weighted mean of U/Pb monazite ages	Scharer et al., 1986
Dinggye	87.625	233	12.5 ± 0.9	Youngest weighted mean of Th/Pb monazite ages	Kali et al., 2010
			13.5 ± 0.3	Weighted mean of Th/Pb monazite ages	Kali et al., 2010

(Table 2 continued)

Region	Longitude (°)	Area (Km^2)	Timing (Ma)	Basis	References
			16.9 ± 0.4	Weighted mean of U/Pb monazite ages	Leloup et al., 2010
			16.0 ± 0.6	Youngest Weighted mean of U/Pb monazite ages	Leloup et al., 2010
Mabja	87.9	106	11.2 ± 0.5	Concordant U/Pb zircon and xenotime age	King et al., 2011
			8.8 ± 0.2	Concordant U/Pb zircon, monazite and xenotime ages	King et al., 2011
			9.2 ± 0.9	Weighted mean of U/Pb monazite ages	Scharer et al., 1986
			9.8 ± 0.7	Weighted mean of U/Pb monazite ages	Scharer et al., 1986
			14.4 ± 0.2	Weighted mean of U/Pb monazite ages	Zhang et al., 2004
			23.1 ± 0.8	Weighed mean of U/Pb zircon ages	Lee et al., 2006
Sikkim	88.6	<10	13.2 ± 0.3	Youngest weighted mean of U/Pb monazite ages	Kellett et al., 2013
			14.5 ± 0.1	Youngest weighted mean of U/Pb/Th monazite ages	Kellett et al., 2013
			14.7 ± 0.1	Youngest weighted mean of U/Pb/Th monazite ages	Kellett et al., 2013
			17.0 ± 1.6	Mean of Th/Pb monazite ages	Edwards et al., 2002, Catlos et al., 2004
Kouwu	88.1	19	14.2 ± 0.2	Weighed mean of U/Pb zircon ages	Lee et al., 2006
			25.4 ± 6.0	Concordia U/Pb zircon age	King et al., 2011
			14.4 ± 0.6	Low intercept U/Pb xenotime age	King et al., 2011
			22.9 ± 0.17	U/Pb monazite age	Wu et al., 1998
Kuday	88.365	132	14.5 ± 0.9	Weighted mean of U/Pb zircon age	King et al., 2011
			16.2 ± 0.4	Weighted mean of U/Pb zircon age	Lee and Whitehouse, 2007

(Table 2 continued)

Region	Longitude (°)	Area (Km^2)	Timing (Ma)	Basis	References
			21.5 ± 0.4	Weighted mean of U/Pb zircon age	Lee and Whitehouse, 2007
			22.6 ± 0.4	Low intercept of U/Pb xenotime age	King et al., 2011
			27.5 ± 1.0	Concordant U/Pb zircon age	King et al., 2011
			27.5 ± 0.5	Weighted mean of U/Pb zircon age	Zhang et al., 2004
			28.1 ± 0.4	Concordant U/Pb zircon age	King et al., 2011
			35.0 ± 0.8	Weighted mean of U/Pb zircon age	Lee and Whitehouse, 2007
Yadong	88.95	281	~22.9	Mean of U/Pb zircon ages	Wu et al., 1998
Wagye La	89.875	125	~11.9	Mean of U/Pb zircon ages	Wu et al., 1998
Ramba	90.04	31	7.6 ± 0.2	Weighted mean of U/Pb zircon ages	Liu et al., 2014
			7.7 ± 0.2	Weighted mean of U/Pb xenotime ages	Liu et al., 2014
			7.9 ± 0.2	Weighted mean of U/Pb xenotime ages	Liu et al., 2014
			8.0 ± 0.5	Weighted mean of U/Pb zircon ages	Liu et al., 2014
			8.1 ± 0.2	Weighted mean of U/Pb monazite ages	Liu et al., 2014
			8.1 ± 0.3	Weighted mean of U/Pb monazite ages	Liu et al., 2014
			8.3 ± 0.5	Weighted mean of U/Pb zircon ages	Liu et al., 2014
			28.2 ± 5.2	Weighted mean of U/Pb zircon ages	Liu et al., 2014
			44.1 ± 0.8	U/Pb zircon age	Liu et al., 2014
			44.3 ± 0.5	U/Pb zircon age	Liu et al., 2014
Masang Kang-Paro	90.175	590	14 – 13	U/Pb monazite ages	Searle and Godin, 2003
			24 – 23	U/Pb monazite ages	Searle and Godin, 2003

(Table 2 continued)

Region	Longitude (°)	Area (Km^2)	Timing (Ma)	Basis	References
Khula Kangri	90.75	1,129	12.5 ± 0.15	Weighted mean of Th/Pb monazite ages	Edwards and Harrison, 1997
Yala Shangbo	92	81	20.3 ± 1.9	Mean of U/Pb zircon ages	Yan et al., 2012

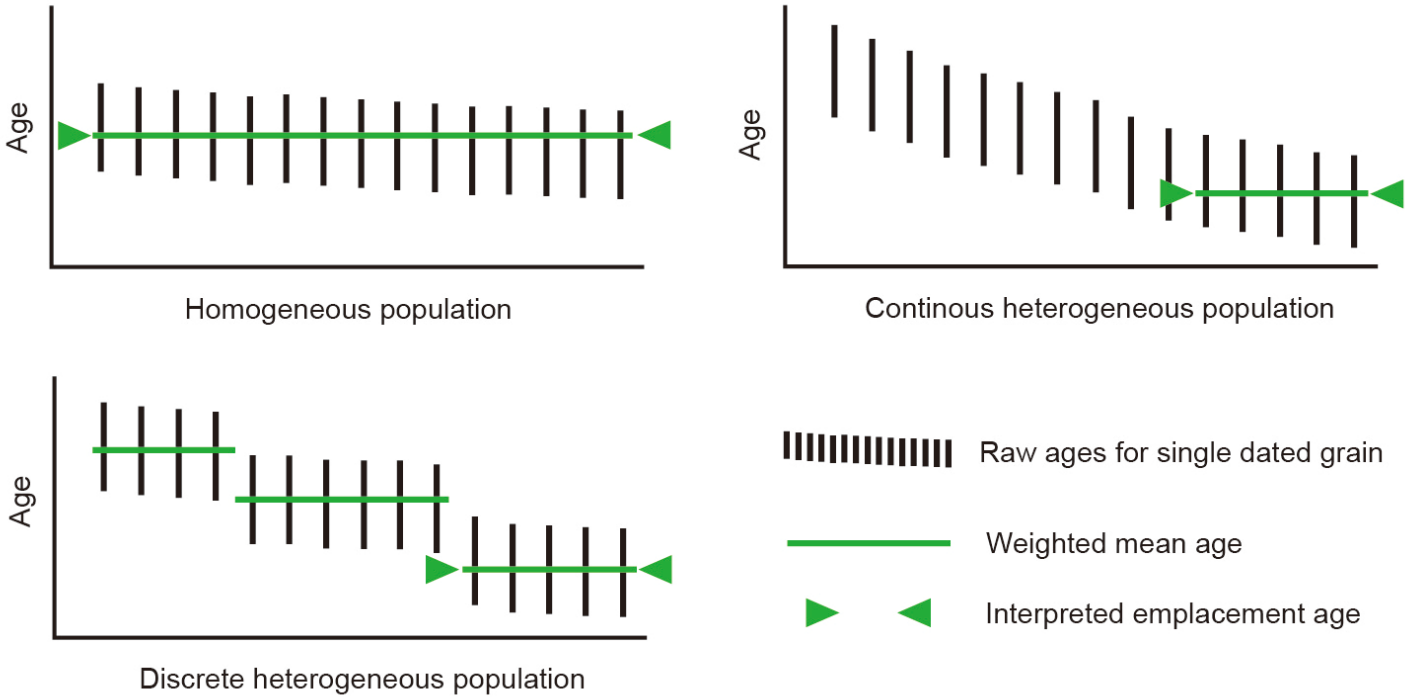

Figure 12. U-(Th-)Pb age patterns and interpretation. The Vertical axis represents raw age population for a single dated result. Green line mark indicates weighted mean ages. For homogenous age population as evidenced by low MSWD, the weighted mean of total population is interpreted to represent the emplacement age for leucogranite. For heterogeneous age population, the weighted mean of youngest cluster is interpreted to suggest the emplacement age.

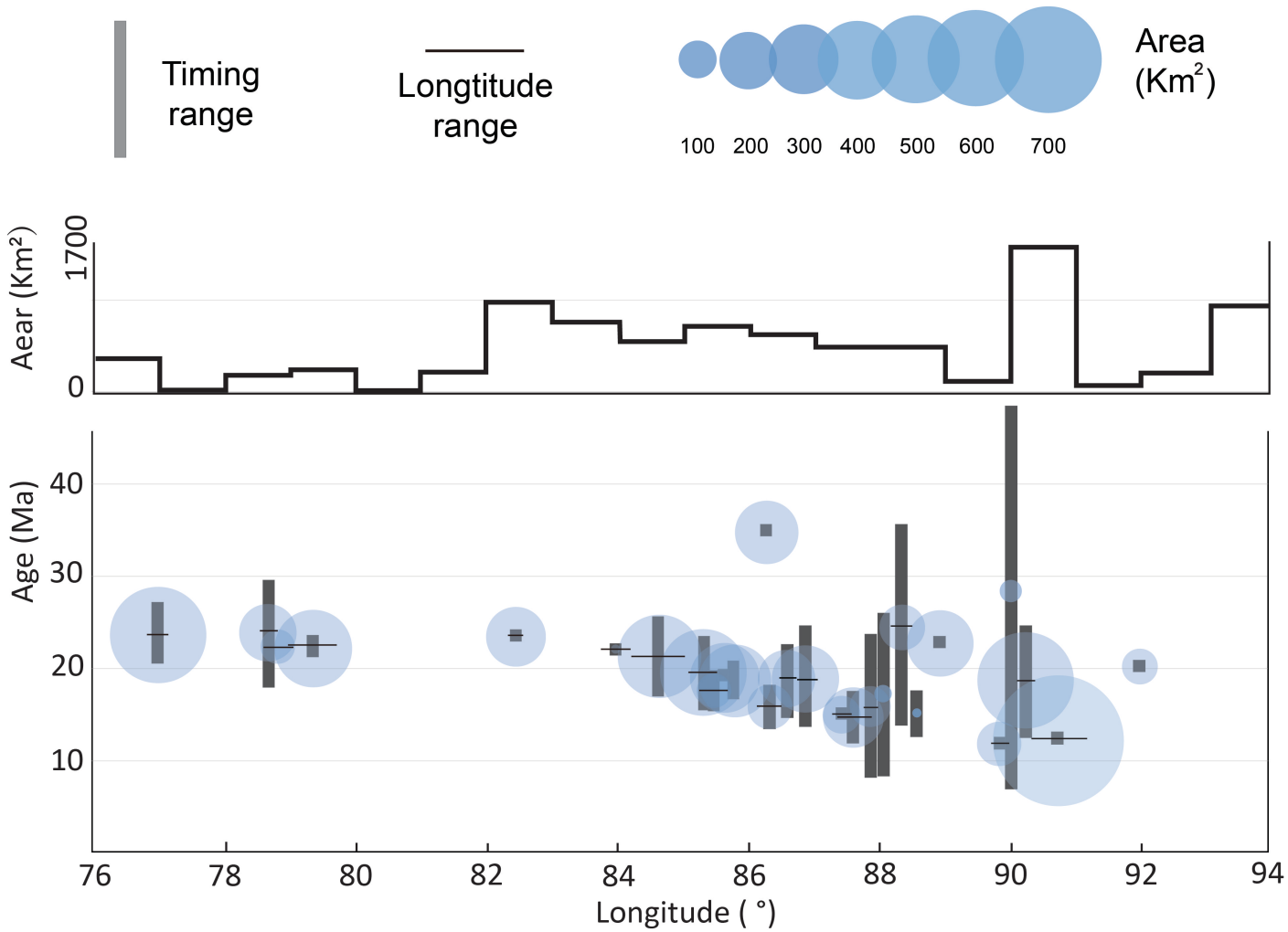

Figure 13. Age and are of leucogranite vs. longitude diagram. The horizontal axis shows the longitude that the leucogranite bodies locate and extend. The vertical axis shows the timing of the leucogranite compiled from the published geochronological work (sources in Table 2). The circles show the estimated areas of the leucogranite bodies. The upper part of the diagram shows the area of leucogranites distributed along per longitude.

emplacement was made, however may represent the emplacement age or pre-date the actual emplacement.

Most leucogranite bodies have a wide range of timing (Figure 14). Experimental petrology demonstrated that the single magmatic event has fast segregation, ascent and emplacement history in Himalaya, so we do not interpret the widespread timing range from single samples to be a long crystallization history (Scaillet and Searle, 2006). Instead, we believe the leucogranite magmatic event has a long history but consists multiple magma pulses (Lee and Whitehouse, 2007; Zhang et al., 2011; Gao et al., 2013; Lederer et al., 2013), which is also suggested by the dense resolution of U/Pb zircon geochronology and thermal modeling in Mt. Caoanne pluton in Elba, Italy (Barboni et al., 2015)

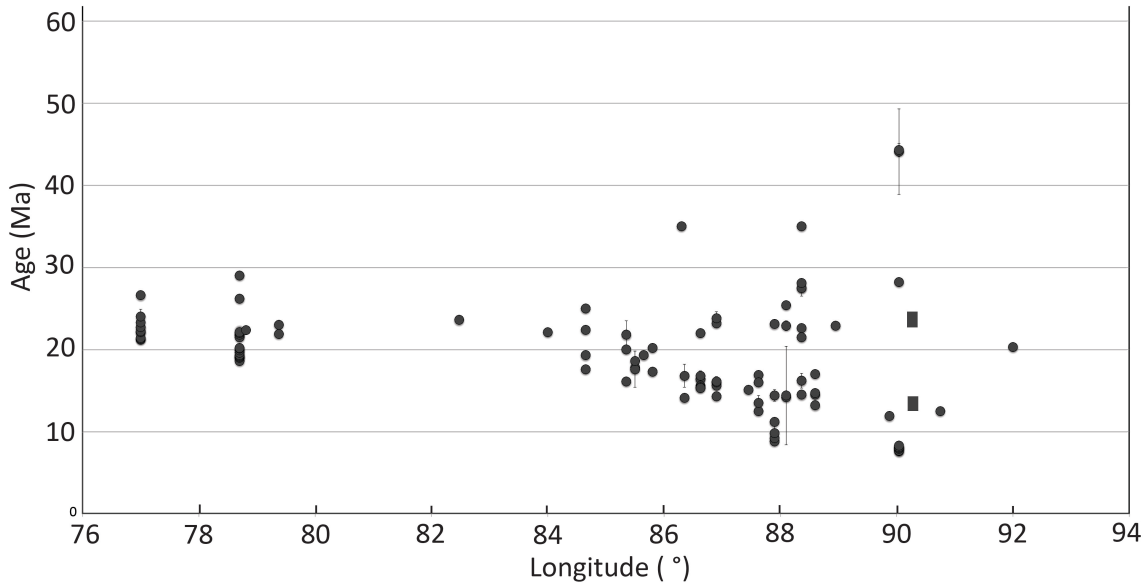

Figure 14. Age of leucogranite vs. longitude diagram. Age data is compiled form published geochronological work (see table 2 for sources). Errors are in 2-σ level. Note that rectangles represent range of multiple age results.

Another difficulty in interpreting crystallization and emplacement age of Himalayan leucogranite is that a single sample sometimes yields a wide range of ages or multiple clusters of

ages that are much greater than the limits of analytical uncertainty. Therefore, those heterogeneous ages should be interpreted with geological meaning. Here, the possibility that older ages indicate the leucogranite crystallization and the younger ages represent later U-Th/Pb system disturbances were excluded, because Lederer et al. (2013) pointed out that Himalayan leucogranite does not contain enough heat for Pb-loss and that later recrystallization from fluid assistance and deformation can be distinguished from X-ray maps. Thus, in case with filed-based evidence that monazite systematics were disturbed or reset by later events, we interpret the younger ages to be reliable crystallization ages. However, in some cases dated zircons may be inherited, and therefore these ages could predate the crystallization.

The geochronological data shows a clear timing variation along the length of the Himalaya. The earliest leucogranite generation occurred prior to 30 Ma in some regions along the Himalayan orogen. The whole orogen experienced leucogranite generation from ca. 30 Ma. The cessation of the leucogranite emplacement occurred earlier, ca. 20 Ma, at the ends of the orogen, and is progressively younger towards the east-central Himalaya with a finial cessation ca. 8 Ma. The propagation of cessation from the western Himalaya to the east-central Himalaya is faster than from the eastern Himalaya to the east-central Himalaya.

4.2 Volume

We mapped the main leucogranite bodies along the orogen and projected them in an equal-area projection in ArcGIS (see Estimated Areas in Table 2, also shown as circles in Figure 14). We employed this as a proxy to examine the amount of leucogranite produced along the orogen through time. Results show that younger leucogranite bodies appear generally larger than older emplaced bodies in any given range sector, and that more leucogranite occurs in the vicinity of the east-central Himalaya whereas less leucogranite appears at the ends of the orogen. These

results are consistent with the prediction of the three-dimensional slab dynamics model that larger leucogranite bodies were produced during or immediately after the slab detachment and that the duplexing of the crystalline core lasted for longer period at east-central Himalaya than at the ends of the orogen.

Here, a map and a cross section of a large leucogranite body intruded at the Leo Pargil dome were presented (Figure 15). In this location, timing and volume of the leucogranite were examined via published geochronological data (Lederer et al., 2013) and outcrop mapping (Langille et al., 2012; Lederer et al., 2013). This site is selected for additional attention because it has received unusually detailed geochronological interrogation by the teams of Langille et al. (2012) and Lederer et al. (2013), allowing for a relatively strong exploration of age vs. volume constraints.

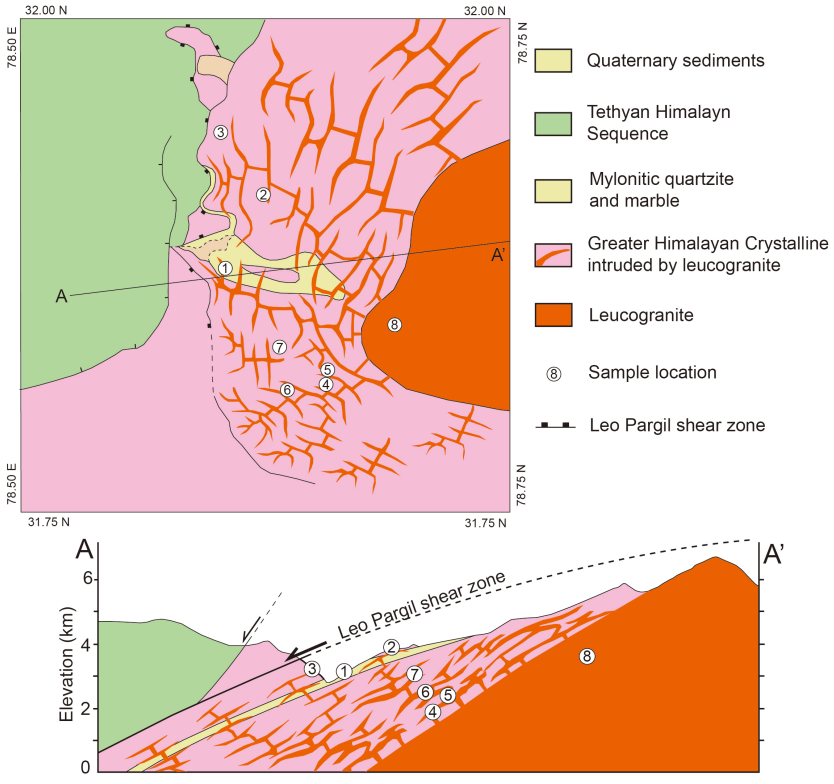

Figure 15. Geological map of the Leo Pargil dome. Modified from Langille et al. (2012) and Lederer et al. (2013).

From the structurally high to low levels, 19 leucogranite samples were dated by monazite grains and produced Th/Pb ages. At location 3, monazites from a thin leucogranite sill (ca. 5 cm) were dated as 29.0 ± 0.2 Ma, and monazites from another thicker leucogranite sill (ca. 20 – 50 cm) were dated as 21.8 ± 0.4 Ma. At location 2, monazites from a 2 m thick leucogranite sill were dated as 26.2 ± 0.2 Ma, and monazite from a 10 cm wide leucogranite dike were dated as 19.6 ± 0.1 Ma. At location 1, two ca.10 cm wide thin leucogranite dikes were dated as 21.5 ± 0.2 Ma and as 19.9 ± 0.1 Ma respectively. At location 7, monazites from an early generation of 10 cm wide thin leucogranite sill were dated as 20.7 ± 0.2 Ma, and monazites from a later thick (somewhere reaches 1 m wide) leucogranite sill were dated as 19.6 ± 0.2 Ma. At location 6, monazites from a 10 to 20 cm wide thin leucogranite vein were dated as 21.7 ± 0.2 Ma. The other three younger leucogranite bodies cut this leucogranite body, and they are: an leucogranite with uncertain width dated as 20.1 ± 0.3 Ma, a ca. 50 cm wide leucogranite vein dated as 19.3 ± 0.2 Ma, and a large leucogranite intrusion, over 1 m wide, dated as 19.2 ± 0.2 Ma. At location 5, monazite from an ca. 50-cm-wide leucogranite dike were dated as 20.2 ± 0.2 Ma; two sets of monazites from an large leucogranite dike (over 1 m wide), which cut the older dike, were dated as 19.0 ± 0.3 Ma and 19.0 ± 0.2 Ma respectively. Another younger generation of thin leucogranite dike, dated as 18.6 ± 0.1 Ma cut the large dike. At location 4, monazites from a 10 to 20 cm wide leucogranite dike were dated as 22.1 ± 0.3 Ma, and monazites from a 50 cm wide leucogranite dike were dated as 19.1 ± 0.3 Ma. At location 8, monazites from a ca. 80 cm wide leucogranite dike were dated as 17.9 ± 0.1 Ma.

At the Leo Pargil dome, the leucogranites were distributed in the following trends: (1) the older generations of leucogranites are generally located at a higher structural level, and the younger generations are generally located at lower structural level (Figures 15, 16); (2) the older

generations are generally small bodies (i.e., 10 to 20 cm wide), while the younger generations are generally larger bodies (i.e., 50-100 cm wide with some dikes wider than 100cm). This regional example matches the predictions of the propagating slab detachment model that in each range sector, early leucogranite bodies are of lesser volume and later ones have greater volume.

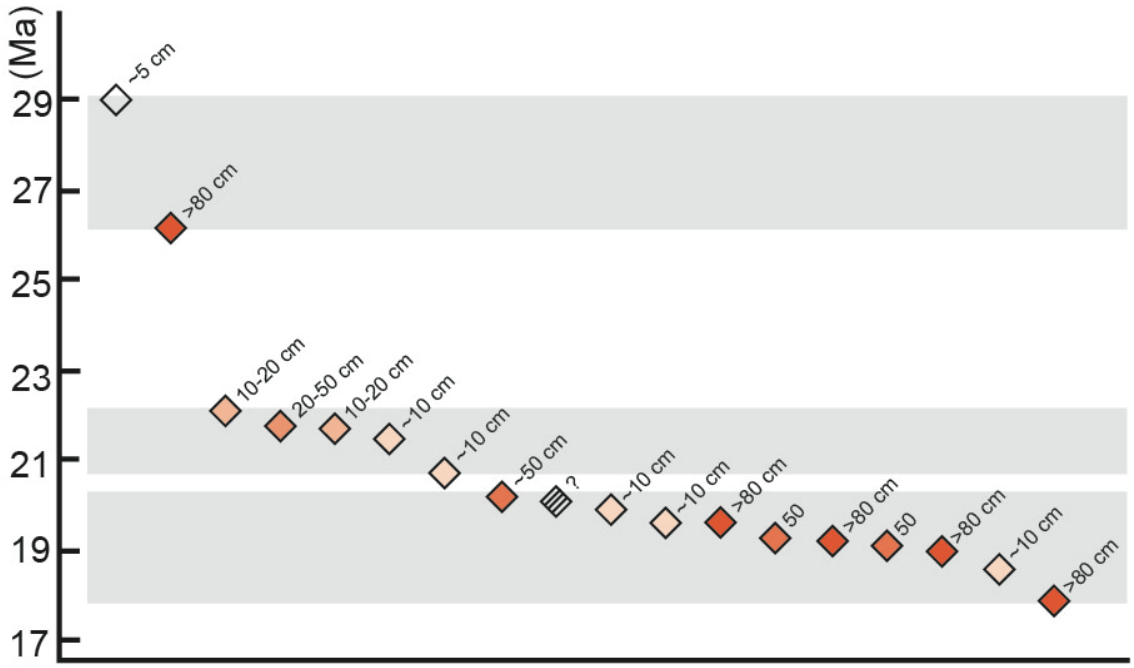

Figure 16. Age and width of leucogranites at Leo Pargil dome. Vertical axis shows the age of dated leucogranite veins/dikes/sills in Leo Pargil dome (data from Lederer et al., 2013). The widths (here regarded as a proxy to indicate volume of different generations) of leucogranites are shown in color code that the larger the leucogranite volumes are, the more saturate the orange color fills are. Three stages with distinctive grey background are shown, and these are: (1) from ca. 29 to ca. 26 Ma, (2) from ca. 22-21 Ma, (3) after ca. 21 Ma. These are interpreted to be the leucogranite generation during slab rollback, Greater Himalayan Crystalline duplexing, and slab detachment respectively. Another interpretation is that first cluster of data points represents the leucogranite generation during rollback, that the following two clusters of data points represent the leucogranite generation during slab detachment, and that data points are not dense enough to reflect the proposed duplexing stage.

CHAPTER 5. CONCLUSIONS

The geochronological data compilations and volume estimates clearly suggest that increasing volumes and younging of leucogranite bodies from the ends of the orogen towards the east-central Himalaya and that younger leucogranite bodies appear generally larger than older emplaced bodies in any given range sector (Figures 13, 14).

These findings are generally consistent with the predictions of the lateral migration of slab detachment model, suggesting that this model offers a reasonable explanation for the spatiotemporal distribution of Himalayan leucogranite: (1) underthrusting prior to ca. 30 Ma and rollback of the Indian slab during ca. 30 to 25 Ma (Webb et al., submitted) produced a small volume of leucogranite melting via burial heating, (2) duplexing contributed to a modest volume of leucogranite melting via shear heating and decompression, and (3) a large volume of leucogranite melting was triggered during or immediately after the Indian slab detachment via rapid decompression in response to the rapid uplift and exhumation (see Figure 17 for variable

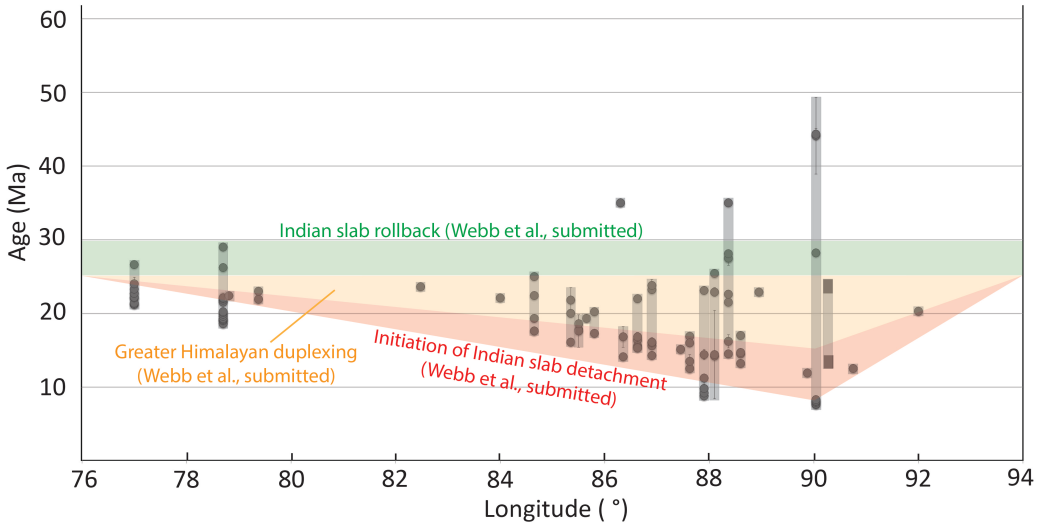

Figure 17. Interpreted spacing and timing for Indian slab dynamics and its control on leucogranite generation. The Indian slab experienced rollback during ca. 30 Ma to ca. 25 Ma. The slab detachment initiated at ca. 20 Ma beneath the ends of the Himalaya and propagated towards the east-central Himalaya.

timing along the strike). The propagation of slab detachment from ends of the orogen towards east-central Himalaya results in the asynchronous cessation of leucogranite generation.

This interpretation prompts a re-evaluation of pre-existing two-dimensional models and confirms that Himalayan mountain building proceeded largely via duplexing, as modulated in three dimensions and time by the dynamics of the subducting Indian plate.

This work admittedly has the following limitations. Our volume estimates are realized by calculating the area of the distinctive leucogranite bodies. The two-dimensional result, without vertical scale, will have limitations on reflecting precise three-dimensional volumes. However, this is currently the best proxy to estimate the volume of the leucogranites along the Himalayan. In addition, because of the limitation on the density of published geochronological data sets and filed mapping sources (and outcrop sources), I cannot analyze the volume of leucogranite produced in different generations on every leucogranite bodies along the strike using the analysis methods that were used to determine the timing-volume relationship at Leo Pargil dome. Lack of dense geochronological data at west-central Himalayan leucogranite weakens the age constraints on the west-central region of the Himalaya. However, the overall temporal constraint is strong and clear.

Further study will attempt to compile geochemical records as another proxy to distinguish the leucogranites generated at as the products of partial melting in response to prograde heating, or retrograde decompression, or both of them, and thus fulfill more comprehensive tests to these models. Compilations of trace elements and REE data sets are necessary to identify which minerals from the crustal source were melting and the degree of their melting, which may potentially distinguishes vapor-present melts and vapor-absent melts.

REFERENCES

Aoya, M., Wallis, S.R., Terada, K., Lee, J., Kawakami, T., Wang, Y. and Heizler, M., 2005, North-south extension in the Tibetan crust triggered by granite emplacement: Geology, v. 33, p. 853-856.

Arita, K., 1983, Origin of the inverted metamorphism of the Lower Himalaya, central Nepal: Tectonophysics, v. 95, p. 43 Harrison, M.T., Grove, M., Mckeegan, K.D., Coath, C.D., Lovera, O.M. and Le Fort, P., 1999b, Origin and episodic emplacement of the Manaslu intrusive complex, central Himalaya: Journal of Petrology, v. 40, p. 3-19.60.

Beaumont, C., Jamieson, R.A., Nguyen, M.H., and Lee, B., 2001, Himalayan tectonics explained by extrusion of a low-viscosity crustal channel coupled to focused surface denudation: Nature, v. 414, p. 738-742.

Burchfiel, B.C., and Royden, L.H., 1985, North-south extension within the convergent Himalayan region: Geology, v. 13, p. 679-682.

Burg, J.P., Brunel, M., Gapais, D., Chen, G.M., and Liu, G.H., 1984, Deformation of leucogranites of the crystalline Main Central Sheet in southern Tibet (China): Journal of Structural Geology, v. 6, p. 535-542.

Carosi, R., Montomoli, C., Rubatto, D. and Visonà, D., 2013, Leucogranite intruding the South Tibetan Detachment in western Nepal: implications for exhumation models in the Himalayas: Terra Nova, v. 25, p. 478-489.

Catlos, E.J., Dubey, C.S., Harrison, T.M. and Edwards, M.A., 2004, Late Miocene movement within the Himalayan Main Central Thrust shear zone, Sikkim, north - east India: Journal of Metamorphic geology, v 22, p. 207-226.

Cottle, J.M., Searle, M.P., Jessup, M.J., Crowley, J.L. and Law, R.D., 2015, Rongbuk re-visited: Geochronology of leucogranites in the footwall of the South Tibetan Detachment System, Everest Region, Southern Tibet: Lithos, v. 227, p. 94-106.

Deniel, C., Vidal, P., Fernandez, A., Le Fort, P. and Peucat, J.J., 1987, Isotopic study of the Manaslu granite (Himalaya, Nepal): inferences on the age and source of Himalayan leucogranites: Contributions to Mineralogy and Petrology, v. 96, p. 78-92.

Edwards, M.A., Catlos, E.J., Harrison, T.M. and Dubey, C.S., 2002, We seek him now, we sought him then: 70 years of constraints on the STDS in Sikkim: Jour. Asian Earth Sci, v 20, p. 11-12.

Edwards, M.A. and Harrison, T.M., 1997, When did the roof collapse? Late Miocene north-south extension in the high Himalaya revealed by Th-Pb monazite dating of the Khula Kangri granite: Geology, v. 25, p. 543-546.

England, P., Le Fort, P., Molnar, P. and Pêcher, A., 1992, Heat sources for Tertiary metamorphism and anatexis in the Annapurna - Manaslu region central Nepal: Journal of Geophysical Research: Solid Earth, v 97, p. 2107-2128.

England, P., Molnar, P., 1993, The interpretation of inverted metamorphic isograds using simple physical calculations: Tectonics v. 12, p. 145-157.

Finch, M., Hasalová, P., Weinberg, R.F. and Fanning, C.M., 2014, Switch from thrusting to normal shearing in the Zanskar shear zone, NW Himalaya: Implications for channel flow. Geological Society of America Bulletin, v. 126, p. 892-924.

Godin, L., Gleeson, T., Searle, M.P., Ullrich, T.D., and Parrish, R.R., 2006b, Locking of southward extrusion in favor of rapid crustal-scale buckling of the Greater Himalayan sequence, Nar valley, central Nepal. In: Law, R.D., Searle, M.P., Godin, L. (Eds.), Channel Flow, Ductile Extrusion and Exhumation in Continental Collision Zones: Geological Society of London Special Publication, v. 268, p. 269-292.

Godin, L., Grujic, D., Law, R.D., and Searle, M.P., 2006a, Channel flow, extrusion and exhumation in continental collision zones: an introduction. In: Law, R.D., Searle, M.P., Godin, L. (Eds.), Channel Flow, Ductile Extrusion and Exhumation in Continental Collision Zones: Geological Society of London Special Publication, v. 268, p. 1-23.

Godin, L., Parrish, R.R., Brown, R.L., and Hodges, K.V., 2001, Crustal thickening leading to exhumation of the Himalayan Metamorphic core of central Nepal: insight from U–Pb Geochronology and Ar-40/Ar-39 Thermochronology: Tectonics, v. 20, p. 729-747.

Groppo, C., Rolfo, F. and Indares, A., 2012, Partial melting in the Higher Himalayan Crystallines of Eastern Nepal: the effect of decompression and implications for the 'Channel Flow'model: Journal of Petrology v. 53, p. 1057-1088.

Grujic, D., Casey, M., Davidson, C., Hollister, L.S., Kundig, R., Pavlis, T., and Schmid, S., 1996, Ductile extrusion of the Higher Himalayan Crystalline in Bhutan: Evidence form quartz microfabrics: Tectonophysics, v. 260, p. 21-43.

Guillot, S. and Le Fort, P., 1995, Geochemical constraints on the bimodal origin of High Himalayan leucogranites: Lithos, v. 35, p. 221-234.

Harris, N., and Massey, J., 1994, Decompression and anatexis of Himalayan metapelites: Tectonics, v. 13, p. 1537-1546.

Harris, N., Massey, J. and Inger, S., 1993, The role of fluids in the formation of High Himalayan leucogranites: Geological Society, London, Special Publications, v 74, p. 391-400.

Harrison, M.T., Grove, M., Mckeegan, K.D., Coath, C.D., Lovera, O.M. and Le Fort, P., 1999a, Origin and episodic emplacement of the Manaslu intrusive complex, central Himalaya: Journal of Petrology, v. 40, p. 3-19.

Harrison, M.T., Grove, M., Mckeegan, K.D., Coath, C.D., Lovera, O.M. and Le Fort, P., 1999b, Origin and episodic emplacement of the Manaslu intrusive complex, central Himalaya: Journal of Petrology, v. 40, p. 3-19.

Harrison, T.M., Lovera, O.M. and Grove, M., 1997, New insights into the origin of two contrasting Himalayan granite belts: Geology, v. 25, p. 899-902.

Harrison, T.M., McKeegan, K.D. and LeFort, P., 1995, Detection of inherited monazite in the Manaslu leucogranite by 208Pb/232Th ion microprobe dating: crystallization age and tectonic implications: Earth and Planetary Science Letters, v. 133, p. 271-282.

He, D., Webb, A.A.G., Larson, K.P., Martin, A.J. and Schmitt, A.K., 2015, Extrusion vs. duplexing models of Himalayan mountain building 3: duplexing dominates from the Oligocene to Present: International Geology Review, v 57, p. 1-27.

Hodges, K.V., 2000, Tectonics of the Himalaya and southern Tibet from two perspectives: Geological Society of America Bulletin, v. 112, p. 324-350.

Hodges, K.V., Hurtado, J.M., and Whipple, K.X., 2001, Southward extrusion of Tibetan crust and its effect on Himalayan tectonics: Tectonics, v. 20, p. 799-809.

Hodges, K.V., Parrish, R.R., Housh, T.B., Lux, D.R., Burchfiel, B.C., Royden, L.H. and Chen, Z., 1992, Simultaneous Miocene extension and shortening in the Himalayan orogen: Science, v 258, p. 1466-1470.

Hodges, K.V., Parrish, R.R. and Searle, M.P., 1996, Tectonic evolution of the central Annapurna range, Nepalese Himalayas: Tectonics, v. 15, p. 1264-1291.

Horton, F., Lee, J., Hacker, B., Bowman-Kamaha'o, M. and Cosca, M., 2015, Himalayan gneiss dome formation in the middle crust and exhumation by normal faulting: New geochronology of Gianbul dome, northwestern India: Geological Society of America Bulletin, v 127, p. 162-180.

Huerta, A.D., Royden, L.H., Hodges, K.V., 1996, The interdependence of deformational and thermal processes in mountain belts: Science, v. 273, p. 637-639.

Kali, E., Leloup, P.H., Arnaud, N., Mahéo, G., Liu, D., Boutonnet, E., Van der Woerd, J., Liu, X., Liu - Zeng, J. and Li, H., 2010, Exhumation history of the deepest central Himalayan rocks, Ama Drime range: Key pressure - temperature - deformation - time constraints on orogenic models: Tectonics, v 29, p. 1-31.

Kawakami, T., Aoya, M., Wallis, S.R., Lee, J., Terada, K., Wang, Y. and Heizler, M., 2007, Contact metamorphism in the Malashan dome, North Himalayan gneiss domes, southern Tibet: an example of shallow extensional tectonics in the Tethys Himalaya: Journal of Metamorphic Geology, v. 25, p. 831-853.

Kellett, D.A., Grujic, D., Coutand, I., Cottle, J. and Mukul, M., 2013, The South Tibetan detachment system facilitates ultra rapid cooling of granulite - facies rocks in Sikkim Himalaya: Tectonics, v. 32, p. 252-270.

King, J., Harris, N., Argles, T., Parrish, R. and Zhang, H., 2011, Contribution of crustal anatexis to the tectonic evolution of Indian crust beneath southern Tibet: Geological Society of America Bulletin, v. 123, p. 218-239.

Kohn, M.J., 2008, P-T-t data from central Nepal support critical taper and repudiate large-scale channel flow of the Greater Himalayan Sequence: Geological Society of America Bulletin, v. 120, p. 259-273.

Larson, K.P., Ambrose, T.K., Webb, A.G., Cottle, J.M. and Shrestha, S., 2015, Reconciling Himalayan midcrustal discontinuities: The Main Central thrust system: Earth and Planetary Science Letters, v. 429, p. 139-146.

Larson, K.P., Gervais, F. and Kellett, D.A., 2013, A P-T-t-D discontinuity in east-central Nepal: Implications for the evolution of the Himalayan mid-crust: Lithos, v. 179, p. 275-292.

Larson, K.P., Godin, L. and Price, R.A., 2010, Relationships between displacement and distortion in orogens: Linking the Himalayan foreland and hinterland in central Nepal: Geological Society of America Bulletin, v. 122, p. 1116-1134.

Le Fort, P., 1973, Les leucogranites à tourmaline de l'Himalaya sur l'exemple du granite du Manaslu (Népal central): Bulletin de la Societe Geologique de France, v. 5-6, p. 555-561.

Le Fort, P., 1975, Himalayas: The collided range. Present knowledge of the continental arc: American Journal of Science, v. A275, p. 1-44.

Le Fort, P., 1981, Manaslu leucogranite: a collision signature of the Himalaya: a model for its genesis and emplacement: Journal of Geophysical Research: Solid Earth, v. 86, p. 10545-10568.

Le Fort, P., Cuney, M., Deniel, C., France-Lanord, C., Sheppard, S.M.F., Upreti, B.N. and Vidal, P., 1987, Crustal generation of the Himalayan leucogranites: Tectonophysics, v. 134, p. 39-57.

Lederer, G.W., Cottle, J.M., Jessup, M.J., Langille, J.M. and Ahmad, T., 2013, Timescales of partial melting in the Himalayan middle crust: insight from the Leo Pargil dome, northwest India: Contributions to Mineralogy and Petrology, v. 166, p. 1415-1441.

Lee, J., McClelland, W., Wang, Y., Blythe, A. and McWilliams, M., 2006. Oligocene-Miocene middle crustal flow in southern Tibet: geochronology of Mabja Dome. Geological Society, London, Special Publications, 268(1), pp.445-469.

Lee, J. and Whitehouse, M.J., 2007, Onset of mid-crustal extensional flow in southern Tibet: Evidence from U/Pb zircon ages: Geology, v. 35, p. 45-48.

Leech, M.L., 2008, Does the Karakoram fault interrupt mid-crustal channel flow in the western Himalaya?: Earth and Planetary Science Letters, v. 276, p. 314-322.

Leloup, P.H., Mahéo, G., Arnaud, N., Kali, E., Boutonnet, E., Liu, D., Xiaohan, L. and Haibing, L., 2010, The South Tibet detachment shear zone in the Dinggye area: Time constraints on extrusion models of the Himalayas: Earth and Planetary Science Letters, v. 292, p. 1-16.

Liao, Z.L., Mo, X.X. and Pan, G.T., 2003, The distribution and tectonic significance of peraluminous granites in southern Xizang: Sedimentary Geology and Tethyan Geology, v. 23, p. 12-20.

Liao, Z.L., Mo, X.X., Pan, G.T., Zhu, D.C., Wang, L.Q., Zhao, Z.D., Geng, Q.R. and Dong, G.C., 2006, Quzhen peraluminous granite, Tibet: Geochemical characteristics and geodynamic significance: Acta Petrologica Sinica, v. 22, p. 845-854.

Liu, Z.C., Wu, F.Y., Ding, L., Liu, X.C., Wang, J.G. and Ji, W.Q., 2015, Highly fractionated Late Eocene (~ 35Ma) leucogranite in the Xiaru Dome, Tethyan Himalaya, South Tibet: Lithos, v. 240, p. 337-354.

Liu, Z.C., Wu, F.Y., Ji, W.Q., Wang, J.G. and Liu, C.Z., 2014, Petrogenesis of the Ramba leucogranite in the Tethyan Himalaya and constraints on the channel flow model: Lithos, v. 208, p. 118-136.

Molnar, P., Chen, W.P. and Padovani, E., 1983, Calculated temperatures in overthrust terrains and possible combinations of heat sources responsible for the Tertiary granites in the Greater Himalaya: Journal of Geophysical Research: Solid Earth, v. 88, p. 6415-6429.

Molnar, P., England, P., 1990, Temperatures, heat flux, and frictional stress near major thrust faults: Journal of Geophysical Research, v. 95, p. 4833-4856.

Murphy, M.A. and Harrison, T.M., 1999, Relationship between leucogranites and the Qomolangma detachment in the Rongbuk Valley, south Tibet: Geology, v. 27, p. 831-834.

Noble, S.R. and Searle, M.P., 1995, Age of crustal melting and leucogranite formation from U-Pb zircon and monazite dating in the western Himalaya, Zanskar, India: Geology, v. 23, p. 1135-1138.

Patiño Douce, A., Harris, N., 1998, Experimental constraints on Himalayan anatexis: Journal of Petrology, v. 39, p. 689-710.

Robinson, D.M., DeCelles, P.G., and Copeland, P., 2006, Tectonic evolution of the Himalayan thrust belt in western Nepal: Implications for channel flow models: Geological Society of America Bulletin, v. 118, p. 865-885.

Robyr, M., Hacker, B.R. and Mattinson, J.M., 2006, Doming in compressional orogenic settings: new geochronological constraints from the NW Himalaya: Tectonics, v. 25, p. 1-19.

Royden, L.H., 1993, The steady state thermal structure of eroding orogenic belts and accretionary prisms: Journal of Geophysical Research, v. 98, p. 4487–4507.

Schärer, U., Xu, R.H. and Allègre, C.J., 1986, U-(Th)-Pb systematics and ages of Himalayan leucogranites, South Tibet: Earth and Planetary Science Letters, v. 77, p.35-48.

Searle, M.P. and Godin, L., 2003, The south Tibetan detachment and the Manaslu Leucogranite: A structural reinterpretation and restoration of the Annapurna - Manaslu Himalaya, Nepal: The Journal of geology, v. 111, p. 505-523.

Searle, M.P., Parrish, R.R., Hodges, K.V., Hurford, A., Ayres, M.W. and Whitehouse, M.J., 1997, Shisha Pangma leucogranite, south Tibetan Himalaya: field relations, geochemistry, age, origin, and emplacement: The Journal of Geology, v. 105, p. 295-318.

Simpson, R.L., Parrish, R.R., Searle, M.P. and Waters, D.J., 2000, Two episodes of monazite crystallization during metamorphism and crustal melting in the Everest region of the Nepalese Himalaya: Geology, v. 28, p. 403-406.

Streule, M.J., Searle, M.P., Waters, D.J. and Horstwood, M.S., 2010, Metamorphism, melting, and channel flow in the Greater Himalayan Sequence and Makalu leucogranite: Constraints from thermobarometry, metamorphic modeling, and U - Pb geochronology: Tectonics, v. 29, p. 1-28.

Thakur, V.C., 1998, Structure of the Chambanappew and position of the main central thrust in Kashmir Himalaya: J. Asian Earth Sci., v. 16, p. 269–282.

Thompson, A.B., 1982, Dehydration melting of pelitic rocks and the generation of H2O-undersaturated granitic liquids: American Journal of Science, v. 282, p. 1567–1595.

Vidal, P., Cocherie, A. and Le Fort, P., 1982, Geochemical investigations of the origin of the Manaslu leucogranite (Himalaya, Nepal): Geochimica et Cosmochimica Acta, v. 46, p. 2279-2292.

Walker, J.D., Martin, M.W., Bowring, S.A., Searle, M.P., Waters, D.J. and Hodges, K.V., 1999, Metamorphism, melting, and extension: age constraints from the High Himalayan slab of southeast Zanskar and northwest Lahaul: The Journal of Geology, v. 107, p. 473-495.

Wang, J.M., Zhang, J.J. and Wang, X.X., 2013, Structural kinematics, metamorphic P–T profiles and zircon geochronology across the Greater Himalayan Crystalline Complex in southcentral Tibet: implication for a revised channel flow: Journal of Metamorphic Geology, v. 31, p. 607-628.

Webb, A.A.G., 2013, Preliminary balanced palinspastic reconstruction of Cenozoic deformation across the Himachal Himalaya (northwestern India): Geosphere, v. 9, p. 572-587.

Webb, A.A.G., Guo, H., Webb, A.A.G., Guo, H., Clift, P.D., Müller, T., Constantino, D., Yin, A., Xu, Z., Cao, H., Wang, Q., Slab dynamics controlled Himalayan mountain building and South Asian monsoon intensification, Submitted to Nature.

Webb, A.A.G., Schmitt, A.K., He, D., and Weigand, E.L., 2011, Structural and geochronological evidence for the leading edge of the Greater Himalayan Crystalline complex in the central Nepal Himalaya: Earth and Planetary Science Letters, v. 304, p. 483-495.

Webb, A.A.G., Yin, A., Harrison, T.M., Célérier, J. and Burgess, W.P., 2007, The leading edge of the Greater Himalayan Crystalline complex revealed in the NW Indian Himalaya: Implications for the evolution of the Himalayan orogeny: Geology, v. 35, p. 955-958.

Wu, C., Nelson, K.D., Wortman, G., Samson, S.D., Yue, Y., Li, J., Kidd, W.S.F. and Edwards, M.A., 1998, Yadong cross structure and South Tibetan Detachment in the east central Himalaya (89°-90° E): Tectonics, v. 17, p. 28-45.

Yan, D.P., Zhou, M.F., Robinson, P.T., Grujic, D., Malpas, J., Kennedy, A. and Reynolds, P.H., 2012, Constraining the mid-crustal channel flow beneath the Tibetan Plateau: data from the Nielaxiongbo gneiss dome, SE Tibet: International Geology Review, v. 54, p. 615-632.

Yin, A., 2006, Cenozoic tectonic evolution of the Himalayan orogen as constrained by along-strike variation of structural geometry, exhumation history, and foreland sedimentation: Earth-Science Reviews, v. 76, p. 1-131.

Yin, A., Harrison, T.M., Murphy, M.A., Grove, M., Nie, S., Ryerson, F.J., Wang, X.F., and Chen, Z.L., 1999, Tertiary deformation history of southeastern and southwestern Tibet during the Indo-Asian collision: Geological Society of America Bulletin, v. 111, p. 1644-1664.

Yin, A., Harrison, T.M., Ryerson, F.J., Chen, W., Kidd, W.S.F., and Copeland, P., 1994, Tertiary structural evolution of the Gangdese thrust system, southeastern Tibet: Journal of Geophysical Research, v. 99, p. 18175-18201.

Zhang, H., Harris, N., Parrish, R., Zhang, L. and Zhao, Z., 2004, U-Pb ages of Kude and Sajia leucogranites in Sajia dome from North Himalaya and their geological implications: Chinese Science Bulletin, v. 49, p. 2087-2092.

Zhang, J., Santosh, M., Wang, X., Guo, L., Yang, X. and Zhang, B., 2012, Tectonics of the northern Himalaya since the India–Asia collision: Gondwana Research, v. 21, p. 939-960.

VITA

Hongcheng Guo was born in Anhui Province, the People's Republic of China in 1994. He completed a Bachelor of Engineering degree in Resource Exploration Engineering in June, 2014, at Hefei University of Technology. Following the graduation, he entered the LSU Graduate School in the Fall semester of 2014 to pursue a Master of Science degree in Geology.